DSpace Institution

DSpace Repository **http://dspace.org**

Physics Thesis and Dissertations

2024-12

Optical Properties of Undoped and Tin (Sn) Doped Indium Oxide (In2o3) Nanoparticles

Alemu, Gebrie

http://ir.bdu.edu.et/handle/123456789/16364

Downloaded from DSpace Repository, DSpace Institution's institutional repository

OPTICAL PROPERTIES OF UNDOPED AND TIN (sn) DOPED INDIUM OXIDE **(In_2O_3)** NANOPARTICLES

A PROJECT WORK SUBMITTED TO MSC PROJECT BY

GEBRIE ALEMU

BAHIR DAR UNIVERSITY

COLLEGE OF SCIENCE

DEPARTMENT OF PHYSICS

ADVISOR: MOGES TSEGA (Ph.D.)

November, 2024

Bahir Dar, Ethiopia

BAHIR DAR UNIVERSITY

COLLEGE OF SCIENCE

DEPARTMENT OF PHYSICS

The undersigned here by certify that they have read and recommend to the College of Natural Science, MSc project entitled "**Optical Properties of Undoped and Tin (S n) Doped Indium Oxide (In_2O_3) Nano-particle**" for the partial fulfillment of the requirements for the Degree of Master of Science in Physics.

Advisor's name: MogesTsega (Ph.D.)

_____ _____

Signature Date

BAHIR DAR UNIVERSITY

COLLEGE OF SCIENCES

DEPARTMENT OF PHYSICS

As members of the board of examining of the final MS Master Project open defense, we certify that we have read and evaluated the Master Project prepared by **GebrieAlemu** under the title "**Optical Properties of Undoped and Tin (Sn) Doped Indium Oxide (In_2O_3) Nano-particle**" and recommended that the Master Project be accepted as fulfilling the Masters requirement for the Degree of Master of Physics (with specialization Solid State Physics).

Advisor	Signature	Date
External examiner	Signature	Date
Internal examiner	Signature	Date
Chairperson	Signature	Date

Table of Contents

Contents Page

Listof Figures

Figure Page

List of Tables

Table Page

ABBREVIATIONS

Effective Mass Approximation
EMA

Full Width Half Maximum
FWHM

Indium Arsenide
InAS

Indium Tin Oxide
ITO

Metal oxide semiconductors
MOS

Photoluninescence spectroscopic
PLC

ACKNOWLEDGEMENT

First of all, I would like to thank the almighty GOD enabling me to accomplish this project. Secondly, I would like to thank my advisor Dr. MogesTsega for his continuous supportive advice throughout my project work. My deepest gratitude is especially intentioned on his marvelous and beloved psychological approach and treatment. Even though he is very busy of many works, he has been providing me encouragement, show me easy technical ways, very deep and line-by-line comments and feedbacks. These things made me strong to accomplish this project. So, I have not enough words to express my deepest gratitude about him in guiding and showing me the ways that I have used to follow the procedures to be a researcher. Thirdly, I would like to thank BDU for the MSc program given to me. Lastly, I would like to say thank you for all guys who initiates me morally to complete this project work.

ABSTRACT

The present project work has mainly focused on optical properties of undoped and tin doped indium oxide (In_2O_3) Nan-particleS. In this project, the band gap, crystallite size and index of refraction of ITO nano-particle were calculated from UV-Vis spectra using Brus model, Deby Scherer's and mos's relation. As the tin concentration increased from 5% to 50%, the calculated energy band gap decreased from 3.726 eV to 3.709 eV and the crystallite size is increased from 18.40 nm to 25.68 nm. The band gap energy of undoped and Sn doped indium oxide (In_2O_3) nano-particle is inversely proportional to the index of refraction calculated by Moss relation formula. So, the calculated refractive index of ITO is increased due to the decrease of band gap energy as the tin concentration increases.

KEY WORDS: Nano-materials, In_2O_3, ITO, Optical properties, Semiconductor, XRD, UV-Vis Spectroscopy, Crystallite structure, .

CHAPTER ONE

INTRODUCTION

1.1. Background of the Study

Over the past decades, nanostructure metal oxide semiconductors (MOSs) have drawn tremendous attention of researchers due to their vast applications in various fields[1-3]. MOS Nano-materials having a Nano size (1–100 nm) exhibit novel features including high surface area, excellent physical and chemical stability and lower material density compared to their bulk counterpart. Among various MOS nano-materials, indium oxide (In_2O_3) has been investigated widely due to its wide band gap, high electrical conductivity, stability and excellent optoelectronic properties[4]. These features of the nano-materials help the researchers to design and fabricate various functional nano-materials (devices) for practical use.

Beginning from the last decade, MOS IO based nano-materials has been studied extensively. Around 54 years ago,o.Bierulagen,et,al., [5] demonstrated that a small fraction of tin (Sn) doping into IO can significantly increase the electrical conductivity and infrared reflectivity without losing optical transparency in visible region. Based on this experimental observation, the tin (Sn) doped indium oxide (In_2O_3) (ITO) becomes an active area of research. Different nanostructure IO based bulk nano-materials such as Nano sheets, nano-wires, nano-particles, quantum dots, single crystals are suitable for potential applications[6-8]. Among these applications, photovoltaic devices, liquid crystal displays, transparent conductive electrode in electronic devices, solar cells and flat panel displays, photo detectors, gas sensors, heat reflecting windows are some of the applications of IO based MOS nano-materials[9-11]

Recently, the rapid increase in production of various electronic/ optoelectronic devices with ITO results a sharp increase in price of indium. In order to minimize the cost without losing its functional properties, studying the optical properties of indium oxide based nano-particle in detail will make the fabrication of the nano-materials easy [12]. As a result, this project will be concerning on the study of optical properties of undoped and tin doped indium oxide (ITO) nano-particle will be helpful as a reading materials for those researchers focusing on ITO nano-particles.

1.2. Statement of the Problem

In a few last decades, Nano-structure Metal Oxide Semiconductors (MOSs) have drawn the attention of many researchers due to their vast applications in various fields. Among these, indium oxide (In_2O_3) is one of the MOSs that has been investigated widely due to its wide band gap, high electrical conductivity, stability and excellent optoelectronic properties. A small amount of tin (Sn) doping into IO can significantly enhance the electrical conductivity and infrared reflectivity without losing its optical transparency in visible region. These optically transparent electrical conducting nano-materials are useful in a variety of applications. Due to its vast technological importance; this project is focused on the study of the optical properties of undoped and tin doped indium oxide nano-particles.

1.3. Significance of the Study

During this time, different types of nano-materials have broadly been used to improve the materials properties including thermal, electrical, mechanical, optoelectronics, corrosion resistant, self-cleaning, and sensing. Nano-materials having a size (1–100 nm) attracted researchers' attention due to their novel features of high surface area, excellent physical and chemical stability, and lower material density compared to their bulk counterpart. These features of the nano-materials help the researchers to design and fabricate various functional devices for practical use. These materials have technological applications in liquid crystal displays, transparent electrodes for solar cells, gas sensors, photo detectors and laser damage resistant coatings in high power laser technology and so on. As a result, this study will help the pupils and the researchers to know more about the optical properties of undoped and tin doped indium oxide nano-particle.

1.4. Objectives of the Study

1.4.1. General Objective

- To review the optical properties of undoped and tin doped indium oxide (In_2O_3) nano-particle.

1.4.2. Specific Objectives

- To calculate the crystallite size and band gap energies of the nano-particle of undopedandtin doped indium oxide (In_2O_3).

- To determine the refractive index of undoped and tin doped indium oxide (ITO) nano-particle.

1.5. Scope of the Study

This project will focus on assessing different optical properties of undoped and tin doped Indium Oxide nano-particles. The project incorporates some mathematical calculations of the optical properties (such as band gap, crystallite size and index of refraction) of pure and tin doped indium oxide (In2O3) nano-particle.

CHAPTER TWO

2. REVIEW LITERATURE

2.1. Semiconductor Materials

Generally, materials are classified in to three groups based on their property of electrical conductivity. The first groups of materials are conductors that can transfer electric current well. Conductors are made from metallic elements. The second groups of materials are insulators which do not conduct electric current totally. Insulators are made from non metal elements.

Semiconductor materials are the third groups of materials for which the electrical conductivity capacity is between conductors and insulators. They are mostly made from group four elements having four valance electrons. Their electrical conductivity increases if their temperature increases. This property is opposite for metallic materials. The conductivity of a semiconductor materials are also affected by impurity elements in addition to temperature. Impurity elements are out of group four elements which are added in to semiconductor material. The electrical and optical properties of semiconductor materials are highly affected by impurities which are added in a precise controlled amount. The process of adding impurities in to pure semi conductor materials is known as doping. Semiconductor materials can be, classified in to two major groups, intrinsic and extrinsic.

Intrinsic semiconductors exhibit a high degree of chemical impurity. Their conductivity is poor and largely temperature dependent. Single crystals of silicon, germanium and gallium arsenide are some common intrinsic semiconductors. Gallium arsenide (GaAs) crystal is a compound semiconductor where as silicon and germanium crystals are pure element semiconductor materials.

Extrinsic semiconductors are technologically more important. They are produced by addition of a small amounts of impurities (atoms of a different element), usually to a concentration of one part in a million in an intrinsic semiconductor. Group three and group five elements are the most common known impurities. Extrinsic semiconductors can be n-type and p- type. If the added impurity to the crystal is donating a free electron to the crystal, the type of extrinsic

semiconductor material is n-type. If the impurity traps electron from the crystal and produces a hole in the crystal, it is called p-type.

2.2. Band Gap of Semiconductor Materials

In semiconductor physics, the band gap of a semiconductor can be two types, a direct band gap or an indirect band gap. The minimum energy state in the conduction band and the maximum energy state in the valence band are each characterized by a certain crystal momentum (k-vector) in the Brillion zone. If the k-vectors are different, the material has an "indirect gap". If the crystal momentum (k-vector) of electrons and holes is the same in both of the conduction band and the valence band, the material has a “direct band gap”. In the direct band gap an electron can directly emit a photon. In an "indirect" gap, a photon cannot be emitted because the electron must pass through an intermediate state and transfer momentum to the crystal lattice.

Examples of direct band gap materials include amorphous silicon and some III-V materials such as InAs and GaAs. Indirect band gap materials include crystalline silicon and Ge. Some III-V materials are indirect band gap as well, for example AlSb.

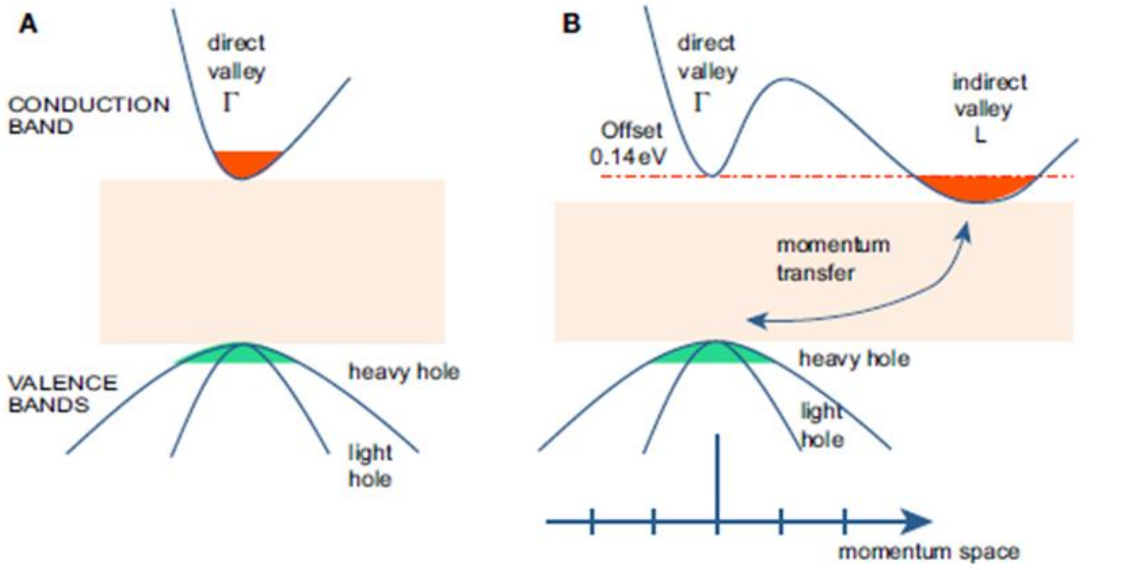

m

Figure 2.1: (A) direct band gap semiconductor and (B) indirect band gap in momentum space[13].

Interactions among electrons, holes, phonons, photons, and other particles are required to satisfy conservation of energy and crystal momentum (i.e., conservation of total k-vector). A photon

with energy near a semiconductor band gap has almost zero momentum. One important process is called radiative recombination, where an electron in the conduction band annihilates a hole in the valence band, releasing the excess energy as a photon. This is possible in a direct band gap semiconductor if the electron has a k vector near the conduction band minimum (the hole will share the same k-vector), but not possible in an indirect band gap semiconductor, as photons cannot carry crystal momentum, and thus conservation of crystal momentum would be violated. For radiative recombination to occur in an indirect band gap material, the process must also involve the absorption or emission of a phonon, where the phonon momentum equals the difference between the electron and hole momentum. It can also, instead, involve a crystallographic defect, which performs essentially the same role. The involvement of the phonon makes this process much less likely to occur in a given span of time, which is why radiativerecombination is far slower in indirect band gap materials than direct band gap ones. This is why light-emitting and laser diodes are almost always made of direct band gap materials, and not indirect band gap ones like silicon.

The fact that radiative recombination is slow in indirect band gap materials also means that, under most circumstances, radiative recombination will be a small proportion of total recombination, with most recombination being non-radiative, taking place at point defects or at grain boundaries. However, if the excited electrons are prevented from reaching these recombination places, they have no choice but to eventually fall back into the valence band by radiative recombination. This can be done by creating a dislocation loop in the material. At the edge of the loop, the planes above and beneath the “dislocation disk” is pulled apart, creating a negative pressure, which raises the energy of the conduction band substantially, with the result that the electrons cannot pass this edge. Provided that the area directly above the dislocation loop is defect-free (no non-radiative recombination possible), the electrons will fall back into the valence shell by radiative recombination, thus emitting light. This is the principle on which "DELEDs" (Dislocation Engineered LEDs) are based.

The exact reverse of radiative recombination is light absorption. For the same reason as above, light with a photon energy close to the band gap can penetrate much farther before being absorbed in an indirect band gap material than a direct band gap one (at least in so far as the light absorption is due to exciting electrons across the band gap). This fact is very important for

photovoltaic (solar cells). Crystalline silicon is the most common solar-cell substrate material, despite the fact that it is indirect-gap and therefore does not absorb light very well. As such, they are typically hundreds of microns thick; thinner wafers would allow much of the light (particularly in longer wavelengths) to simply pass through..

The absorption spectrum of an indirect band gap material usually depends more on temperature than that of a direct material, because at low temperatures there are fewer phonons, and therefore it is less likely that a photon and phonon can be simultaneously absorbed to create an indirect transition. For example, silicon is opaque to visible light at room temperature, but transparent to red light at liquid helium temperatures, because red photons can only be absorbed in an indirect transition.

2.3. Structure and Optical Properties of Indium Oxide (In_2O_3) Nano-particle

2.3.1. Structural study of Indium Oxide (In_2O_3) Nano-particle

Indium (III) oxide (In_2O_3) is a chemical compound which is an amphoteric oxide of indium. Amorphous indium oxide is insoluble in water but soluble in acids, whereas crystalline indium oxide is insoluble in both water and acids. The crystalline form exists in two phases, the cubic (bixbyite type) [14] and rhombohedral (corundum type). Both phases have a band gap of about 3 eV[15,16].

The rhombohedral phase is produced at high temperatures and pressures or when using non-equilibrium growth methods[17]. It has a space group R3c No. 167, Pearson symbol hR30, a = 0.5487 nm, b = 0.5487 nm, c = 1.4510 nm, Z = 6 and calculated density 7.31 g/cm^3[18].

Indium oxide can serve as a semiconductor material, forming hetero junctions with p-InP, n-GaAs, n-Si, and other materials. A layer of indium oxide on a silicon substrate can be deposited from an indium tri chloride solution, a method useful for manufacture of solar cells[19]. Indium oxide is used in some types of batteries, thin films infrared reflectors transparent for visible light (hot mirrors), some optical coatings, and some antistatic coatings. In combination with tin dioxide, indium oxide forms indium tin oxide (also called tin doped indium oxide or ITO), a material used for transparent conductive coatings. In semiconductors, indium oxide can be used as an n-type semiconductor used as a resistive element in integrated circuits.

The structure of the In_2O_3sample was studied by XRD. The XRD patterns of the In_2O_3 samples are shown in Figure 2.2 All of the detectable peaks can be indexed as the In_2O_3 cubic structure in the standard data (JCPDS: 71-2195).

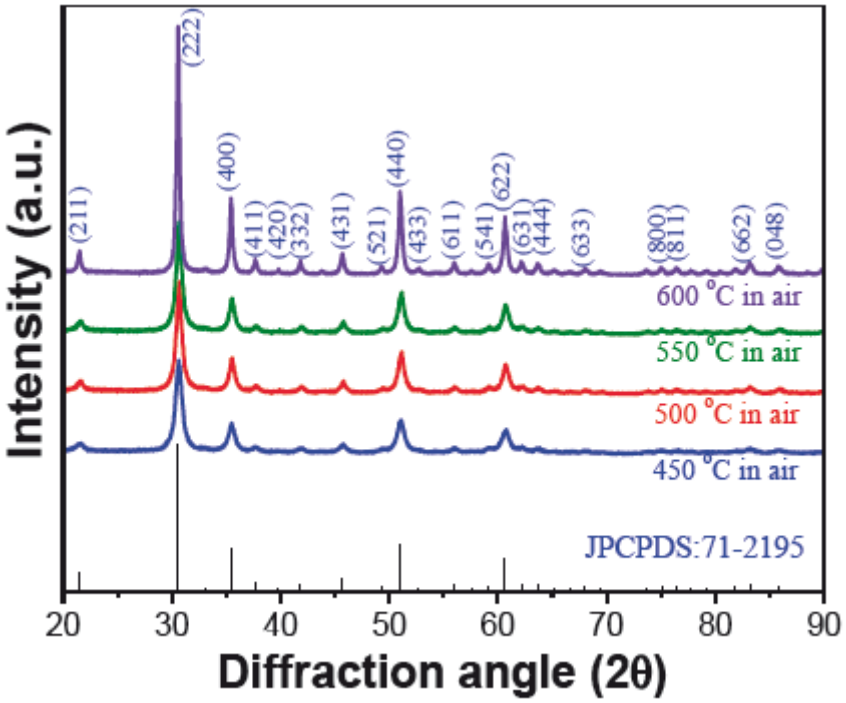

Figure 2.2: XRD patterns of In_2O_3nano-particles calcined in air for 2 h at 450°C, 500°C, 550 °C and 600°C[20].

The cubic lattice parameters *a*, obtained from the XRD spectra are 1.0099, 1.0092, 1.0122 and 1.0119 nm for In_2O_3samples calcined at 450, 500, 550 and 600°C, respectively. These values are approaches to those of lattice constant *a* = 1.0117 nm in the standard data (JCPDS: 71-2195). The crystallite sizes (*D*) of the powders were estimated from X-ray line broadening using debyScherer's equation.

$$D = \frac{0.89\lambda}{\beta Cos(\theta)} \qquad (2.1)$$

where λ is the wavelength of the X-ray radiation, *K* is a constant taken as 0.89, θ is the diffraction angle, β is the full width at half maximum (FWHM) for In_2O_3 samples calcined at 450°C, 500°C, 550°C, and 600°C, respectively. The crystallite sizes and lattice parameters of In_2O_3 samples are summarized in Table 2.1.

Table 2.1: Summary of crystallite sizes from XRD cubic lattice constant and the band gap (E_g) of the nano-crystalline In_2O_3 samples calcined in air at different temperatures for 2h.

In_2O_3 sample	Average crystallite size (D) (nm)	Estimated band gap (eV)	Cubic Lattice Parameter (a) (nm)
Calcined at 400°C	12.1	3.93	1.0099
Calcined at 500°C	13.7	3.90	1.0092
Calcined at 550°C	17.1	3.70	1.0122
Calcined at 600°C	23.7	3.82	1.0119

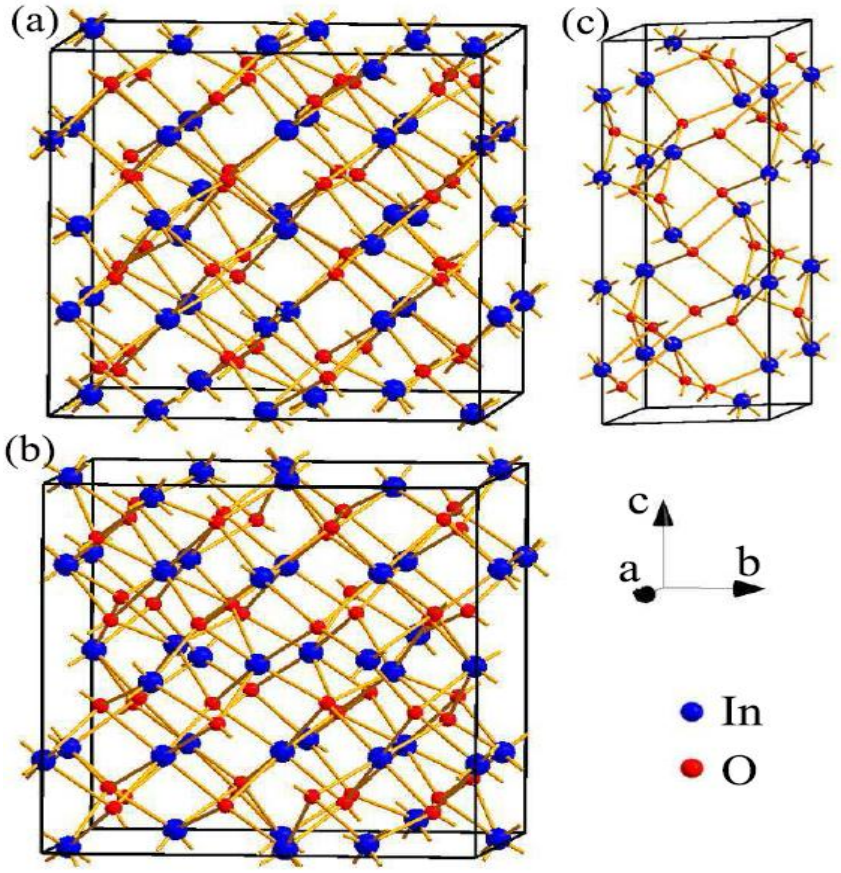

Figure 2.3: Crystal structures of (a) In_2O_3-I, (b) In_2O_3-II, and In_2O_3-III[21].

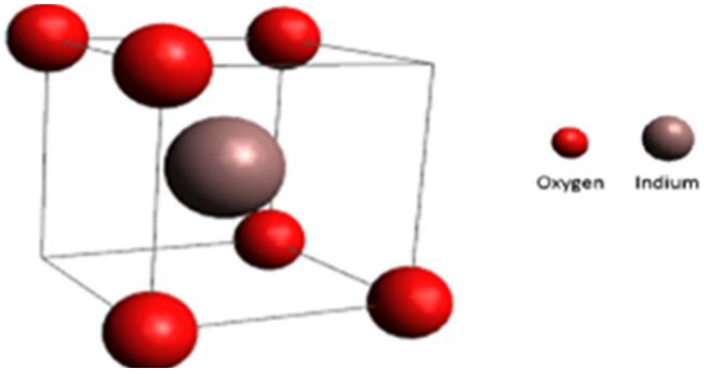

Figure 2.4: Lattice structure of Undoped Indium Oxide[22].

2.3.2. Optical properties of Indium oxide (In_2O_3) Nano-particle

The optical properties of semiconductor material are the necessary information for its application in solar cell. One of the parameter which affects the material optical properties is the band gap energy. The value of band gap energy can be found from experimental data of UV-Vis absorbance spectrum by doing three steps, i.e. curve smoothing, baseline arrangement data value

and the calculation of the band gap energy using Tauc plot method[19]. Indium oxide (In_2O_3) is a wide band gap (3.5 eV–3.75 eV) n-type semiconductor. It has interesting properties such as high transparency to visible light, high electrical conductivity, and strong interaction between certain poisonous gas molecules and its surfaces. These properties make In_2O_3 an interesting material for a variety of applications, including solar cells, panel displays, organic light emitting diodes, photo catalysts, architectural glasses, field emission. Its nano-particle is an important n-type direct band-gap transparent semiconductor around (3.75 eV)[23].

The optical properties of In_2O_3nano-particles were studied by UV-Visible absorption spectroscopy. The absorbance spectra of In_2O_3nano-particles have been shown in the Fig. 2, where the absorbance peak of In_2O_3 was found at 321.9 nm. The absorbance peak depends on the different factors such as crystallite size, band gap, and oxygen vacancies and others. The direct band gap energy (E_g) of the samples is determined by fitting the absorption data to the direct transition equation.

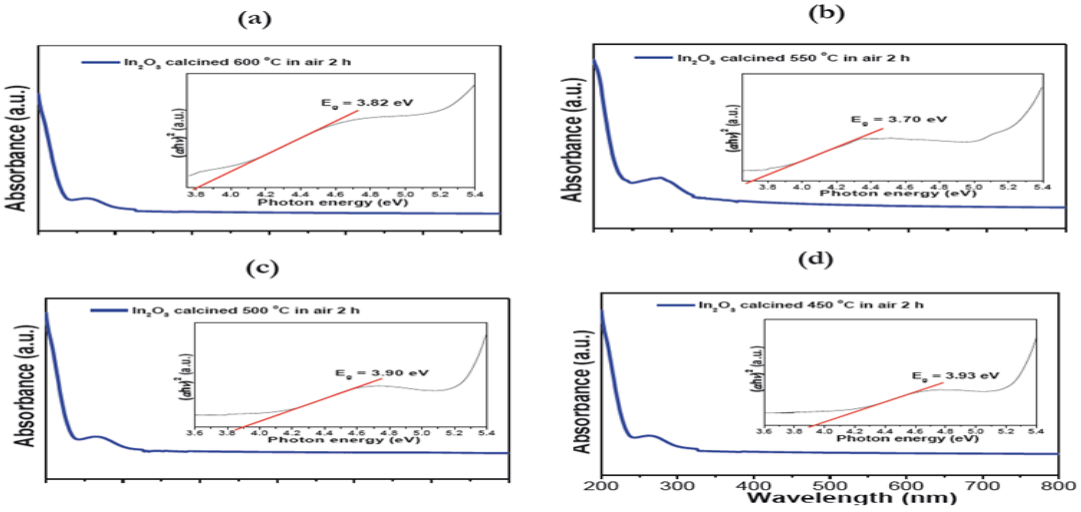

Figure 2.5: Room temperature optical absorbance spectra of In_2O_3samples calcined in air for 2 h at (a) 450°C, (b) 500°C, (c) 550°C and (d) 600°C[19].

The Tauc plot is firstly introduced by Tauc in 1966 when he calculated the band gap energy of amorphous germanium by using the data of absorbance spectrum. This method is based on assumption that the energy is dependent on absorbance coefficient α. This method is then further developed by Davis and Mott for semiconductor material. They found that optical absorbance is

depending on the difference between photon energy and band gap energy. The Tauc equation for semiconductor material is given by

$$(\alpha h\upsilon)^{\frac{1}{n}} = B(h\upsilon - E_g) \quad (2.2)$$

wherehis Plank constant, υ is photon frequency, $E_g$is band gap energy, B is a constant, n is a factor which depend on electron transition property, and α is absorbance coefficient. The value of nis ½ and 2 for direct and indirect band gap transition, respectively. The absorbance coefficient is calculated by

$$\alpha = \frac{\ln(10)A}{l} \quad (2.3)$$

WhereAis absorbance and l is the thickness of the material in centimeter. The determination of band gap energy by using Tauc plot is done by plotting the value of $(\alpha h\upsilon)^{1/n}$withhυ, then followed by taking the extrapolation in the linear area across the energy axis in the corresponding graph. The intersection with energy-axis is the estimation of the corresponding energy gap.

2.4. Structural and Optical Study of Tin (Sn) Doped Indium Oxide (In_2O_3) Nano-particle

2.4.1.Structural Properties of Tin (Sn) Doped Indium Oxide In_2O_3 Nano-particle

2.4.1.1. XRD Analysis

The synthesized ITO NPs were characterized using various characterization techniques. The crystal orientation of the ITO NPs was examined by X-ray diffraction (XRD) (Model: Rigako, smart lab, Japan, MonochromatizedCuKα radiation with Ni filter) operated at 40 kV, 20 mA with CuKα (λ=1.542 Å) radiation as an X-ray source configured in symmetrical θ-2θ mode[24].

The atomistic structure of a unit-cell of ITO resembles that of Indium Oxide (In_2O_3), with the latter being an ionically bound semiconducting oxide, which crystallizes in a cubic bixbyite-type structure with a space group Ia3 and a lattice constant of 10.118 nm[25]. The unit cell of ITO contains 80 atoms, and the Indium cat ions are located in two different six-fold-coordinated sites. One fourth of the cat ions are located in trigonally compressed octahedral, referred as b sites (In-

O distance: 2.18Å), while the remaining three quarters are located on highly distorted octahedral d sites (set of three In-O distances: 2.13, 2.19 and 2.23Å)[26]. As Fig. 1a & b, indium atoms, on both b and d sites, reside at the center of a distorted cube with the six corners occupied by oxygen atoms, while the remaining two corners are empty. In the case of the b sites, oxygen vacancies are located along the body diagonal; for the d site they are located along a face diagonal[26]. Figure 1c shows Tin (Sn) doping sites in an indium oxide lattice, where the Sn atom occupies an interstitial site and contributes an electron (i.e., a donor), making the doped indium oxide into indium tin oxide.

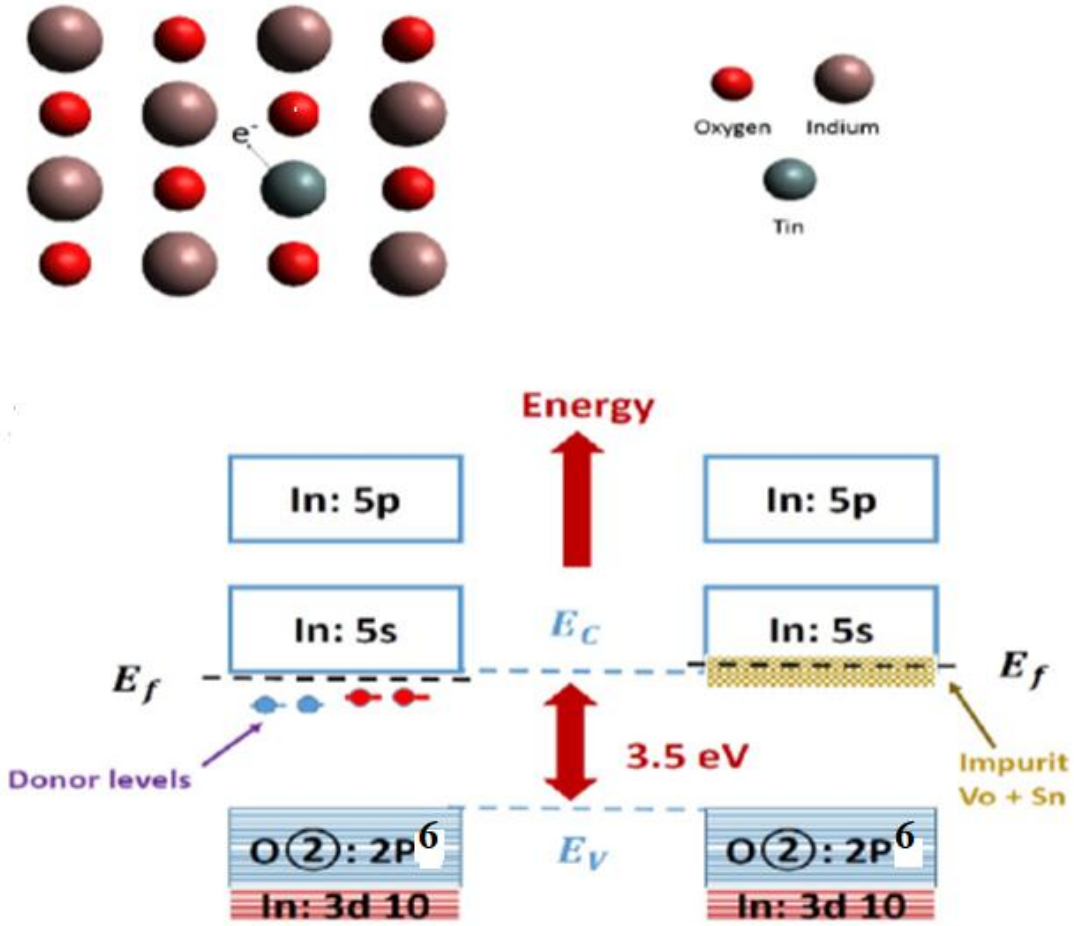

Figure 2.6: Lattice structure of Tin doped Indium Oxide[22].

The XRD patterns of ITO NPs are shown in Fig.2.6. The diffracted peaks indexed at 21.31°(211), 30.4°(222), 35.3°(400), 37.6°(411), 41.7°(322), 45.57°(431), 50.8°(440), and 60.5°(622) correspond to cubic bixbyite (JCPDS 06-0416) structure of ITO NPs. A strong peak was observed in all the samples at 2θ = 30.4° and corresponds to ITO (222) phase[24]. The peak intensity (222) increases as the tin (Sn) concentration increases and the average lattice parameter was calculated and found to be 10.16 Å. The crystallite size (D) of the nano-particle is determined from major peak at 2Θ and equal which is based on Scherer's formula [25]given by;

$$D = \frac{k\lambda}{\beta \cos(\theta)} \tag{2.3}$$

Where k is a correction factor=0.89 ≈ 0.9, β is the full width at half maximum (FWHM) in radian. It is clear that the addition ratios did not change the direction of crystalline growth of the dominant planes (preferred orientation), where growth continues towards (222) direction for In_2O_3, which is attributable to the Drift model[26]. An increase in the full width at half maximum (FWHM) and which consequently leads to a decrease in grain size, according to Scherer's formula with increasing in the addition ratio with Sn as a comparison of pure Indium oxide nano-material, which indicates that the deposited atoms of these nano-particle going towards nano structure.

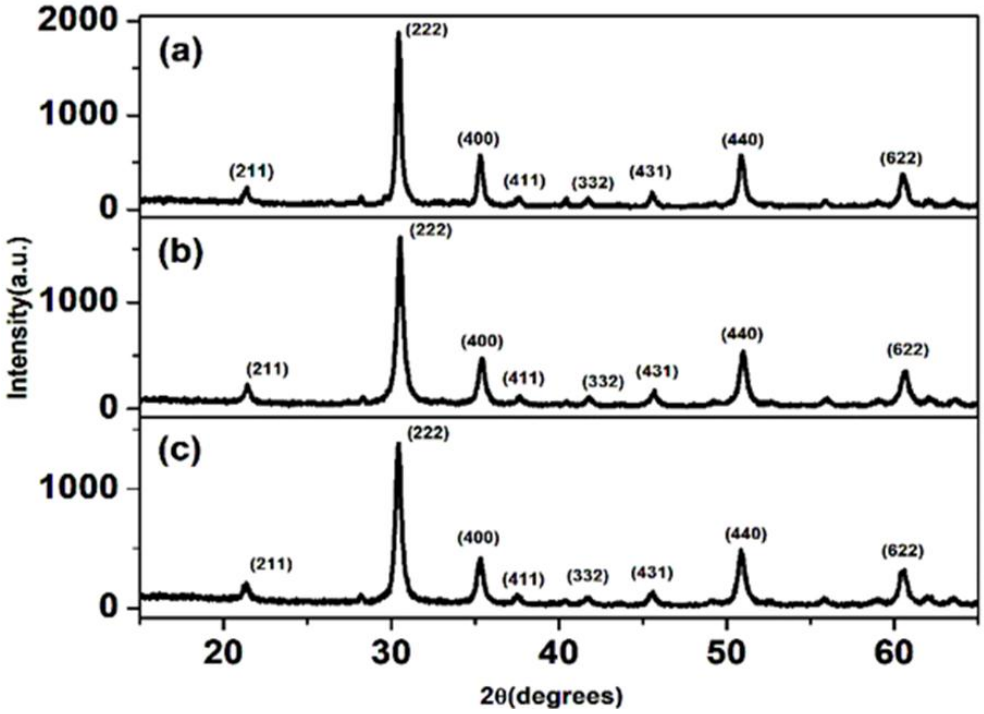

Figure 2.7: XRD patterns of ITO NPs with (a) ITO 5:5 (b) ITO 9:1 (c) ITO 9.5:0.5[24].

Lattice strain decreases as tin (Sn) concentration increases because of an increase in grain size. The absence of SnO_2 peaks (Fig. 2.6) indicates the complete doping of Sn^{4+} ions into the In_2O_3 lattice. Oxygen vacancies usually occupy the (400) plane and are not well occupied in the (222) plane. As it was also observed from XRD spectra, the intensity of the (400) plane increases as tin (Sn) concentration increases resulting in higher oxygen vacancies[24]. The intensity ratio of $I_{(400)}$ /$I_{(222)}$ plane for different Sn concentration is 30.86%, 30.48% and 29.85% for ITO 5:5, ITO 9:1 and ITO 9.5:0.5, respectively. As tin (Sn) concentration increases, the ITO nano-particles will be oriented towards the (222) plane and the I_{222} peak shifts towards a small shift toward a small angle of diffraction 2θ, (to the left of diagram), causing compression in the unit cell because of the ionic radius of the element Sn (0.69Å) smaller than the In (0.80Å), which leads to the atoms of Sn take up substitution sites in order of Indium crystalline lattice as shown in Fig.2.7[24].

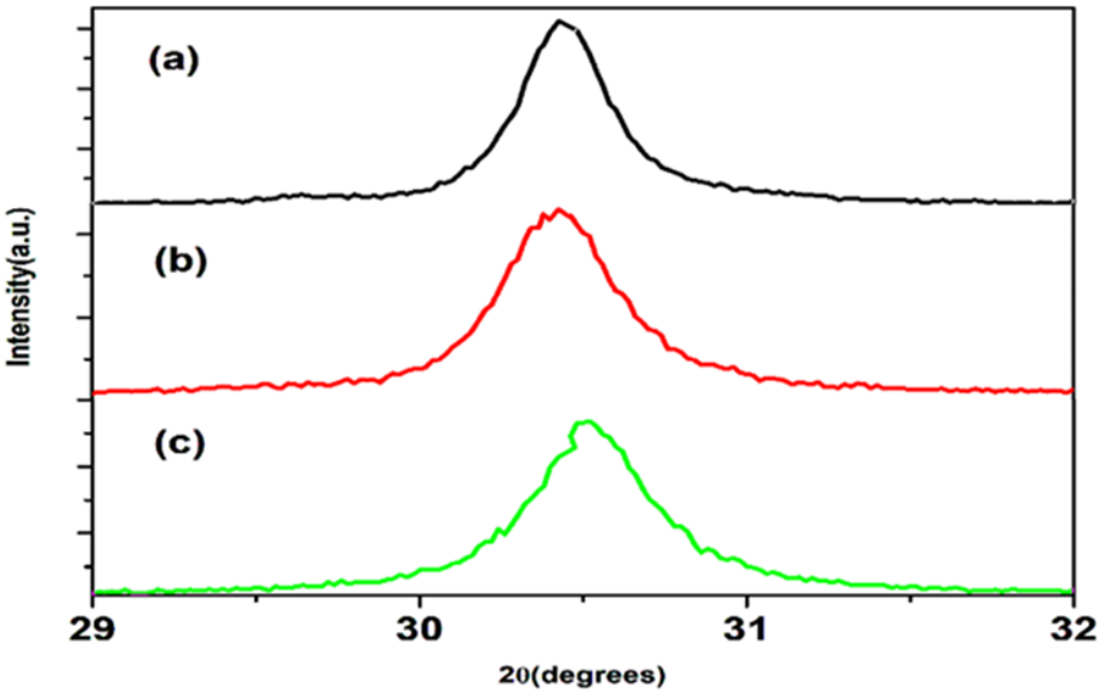

Figure 2.8**:** Shift in I_{222} peak for different ITO NPs with (a) ITO 5:5 (b) ITO 9:1 (c) ITO 9.5:0.5[24].

The ITO NPs with less tin (Sn) content exhibits spongy and more porous structures. As the tin (Sn) concentration increases stuffiness decreases. The less doped ITO NPs appear less dense as it has more pores and cavities. Therefore, more charge carriers are trapped in pores and cavities affecting the conductivity of ITO NPs[24]. It was observed that the Full width at half maximum

(FWHM, β) decreases with an increase in tin (Sn) concentration (Table 1), which indicates an increase in crystallite size. This shows that Sn concentration is an important parameter that influences the crystallinity of ITO NPs.

Table 2.2: Average crystallite size and lattice strain of ITO NPs

ITO Sample of In_2O_3 : Sn	Peak Position at 2θ (degrees)	Peak Position at 2θ (radians)	(hkl)	FWHM (10^{-3}rad)	Average crystallite size (D) (nm)	Average Lattice Strain (ε) (10^{-4})	Lattice Parameter (Å) (Cubic bixbyte)
	30.52	0.5326	(222)	7.82	21.22	5.33	10.14
9.5:0.5	35.40		(400)	7.8			10.16
	50.88		(440)	8.3			10.13
	60.52		(622)	9.3			10.13
	30.43	0.5311	(222)	7.1	27.62	1.91	10.17
9:1	35.39		(400)	7.2			10.12
	50.98		(440)	8.8			10.12
	60.62		(622)	9.4			10.12
	30.42	0.5309	(222)	5.6	35.39	1.24	10.18
5:5	35.31		(400)	5.8			10.16
	50.89		(440)	6.9			10.13
	60.54		(622)	7.6			10.13

2.4.2. Optical Properties of Tin (Sn) Doped Indium Oxide (In_2O_3) Nano-particle

2.4.2.1. UV-Vis Spectroscopy Analysis

Indium tin oxide (ITO) is one of the most widely used transparent conducting oxides because of its optical transparency, electrical conductivity, chemical resistance to moisture and the ease with

which it can be deposited as a nano-material[27]. It is transparent and colorless in thin layers, where as in bulk form it is yellowish to gray. In the infrared region of light spectrum, it acts as a metal-like mirror[27].

When light is incident on a material, a part of it is transmitted (T) through the material, a part of it is reflected (R) and the rest is absorbed by the material. The absorption spectrum of the sample indicates the band structure of solid, energy gap between the valance band and conduction band, the nature of transition (allowed, forbidden, direct and indirect), etc.

Optical absorption is described quantitatively by the absorption co-efficient, α. The α is the fraction of incident light intensity decreased per unit distance in an absorbing medium and it can be given as,

$$I = I_0 \exp(-\alpha x) \tag{2.4}$$

Where 'I_0'is the intensity of incident light, 'x' is the thickness of the material and 'I' is the transmitted light intensity. In an absorbing medium, α is related to the refractive index and the wavelength of the incident light. The refractive index (n) is expressed as,

$$n = n_r - ik \tag{2.5}$$

Where, n_r is the real part of the refractive index and k is called the extinction coefficient. The α of the medium at a given wavelength can be related with the extinction coefficient by,

$$\alpha = \frac{4\pi k}{\lambda} \tag{2.6}$$

UV-Vis spectroscopy (Model UV-3092) with wavelength ranges from 200 to 900 nm was used for optical studies. Pure powder barium sulfate (BaSO4) was used as a standard for background measurement. The ITO NPs were added into the sample holder and then measured using a UV-Vis spectroscopy equipped with an integrated sphere accessory. The optical absorption (A) is related to a semiconductor band gap by the equation;

$$\alpha h\upsilon = A(h\upsilon - E_g)^n \tag{2.7}$$

Where hυ is the photon energy, α is the absorption coefficient, E_g is the band gap, A is constant, n = 1/2 for direct band gap and n=2 for indirect band gap materials. The optical absorption coefficient (α) can be related to the transmittance (T) of a sample with thickness (t) by the equation;

$$\alpha = \frac{2.303}{t} \log\left(\frac{1}{T}\right) \tag{2.8}$$

An ideal transparent material has minimum absorption in near ultraviolet (UV), visible and near infrared (NIR) region. Different types of optical absorption like fundamental absorption, impurity absorption, free carrier absorption, intra band transitions, exciting absorption, and donor–acceptor transitions can occur in a

semiconductor[15]. In the case of the fundamental absorption mechanism involving a direct transition from the valence to the conduction band, the absorption coefficient α for $E>E_g$, i.e. $\lambda<\lambda_g$ is given by;

$$\alpha(E) = \frac{A}{E}\left(E - E_g\right)^{\frac{1}{2}} \tag{2.9}$$

Where 'E', 'E_g' and 'A' are photon energy, band gap energy and a proportionality constant respectively.

2.4.2.1.1. The optical energy band gap

The optical band gap of ITO nano-particle is compared with the band gap value for undoped indium oxide from the plot of $(\alpha h\upsilon)^2$ versus photon energy ($h\upsilon$) according to Tauc's formula which is given by Eq. (2.10) for direct band gap semiconductors[23],

$$(\alpha h\upsilon)^2 = A\left(h\upsilon - E_g\right) \tag{2.10}$$

Where α is the absorption coefficient, A is a constant, E_g is the optical energy gap, υ is the incident photon frequency, t is thickness of the quartz cuvette and h is Planck constant.

The band gap of ITO NPs could also be determined by diffuse reflectance spectroscopy using Kubelka-Munk function described [24]in eq. (2.11).

$$F(R) = \frac{(1-R)^2}{2R} \tag{2.11}$$

Where R is reflectance. The energy of photon E is calculated from eq. (2.12) which is given by;

$$E = \frac{hc}{\lambda} = h\upsilon \tag{2.12}$$

where h is Planck constant ($6.63x10^{-34}$Js), C is the speed of light in vacuum ($3x10^{8}$ m/s), λ is the wavelength of photon and ν is the frequency (Hz), respectively[24].

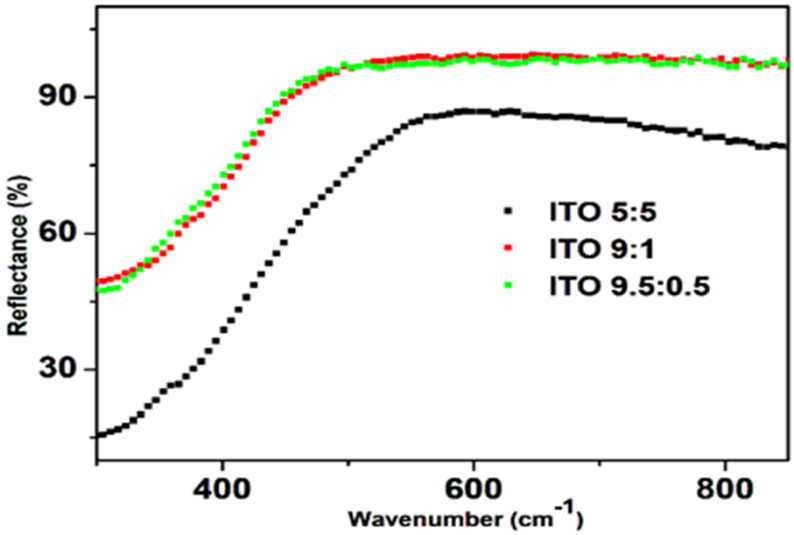

Figure 2.9 **:** Reflectance spectrum of ITO NPs[24].

The plots of energy band gap were obtained using Kubelka-Munk function and photon energy which are shown in Fig. 2.9. The measured energy band gap was in the range of 2.98 to 3.21 eV for synthesized ITO NPs. A larger energy band gap was obtained for small values of I_{400}/I_{222} ratio. As tin (Sn) concentration increases, the band gap energy decreases due to an increase in grain size and a decrease in the grain boundary. This requires less excitation energy for electrons to jump from one grain to another. As tin (Sn) concentration decreases, fewer oxygen vacancies are formed in the ITO NPs which leads to a decrease in carrier concentration. Due to this, band gap energy is shifted to a higher value because of conduction band which is filled partially by carriers[24].

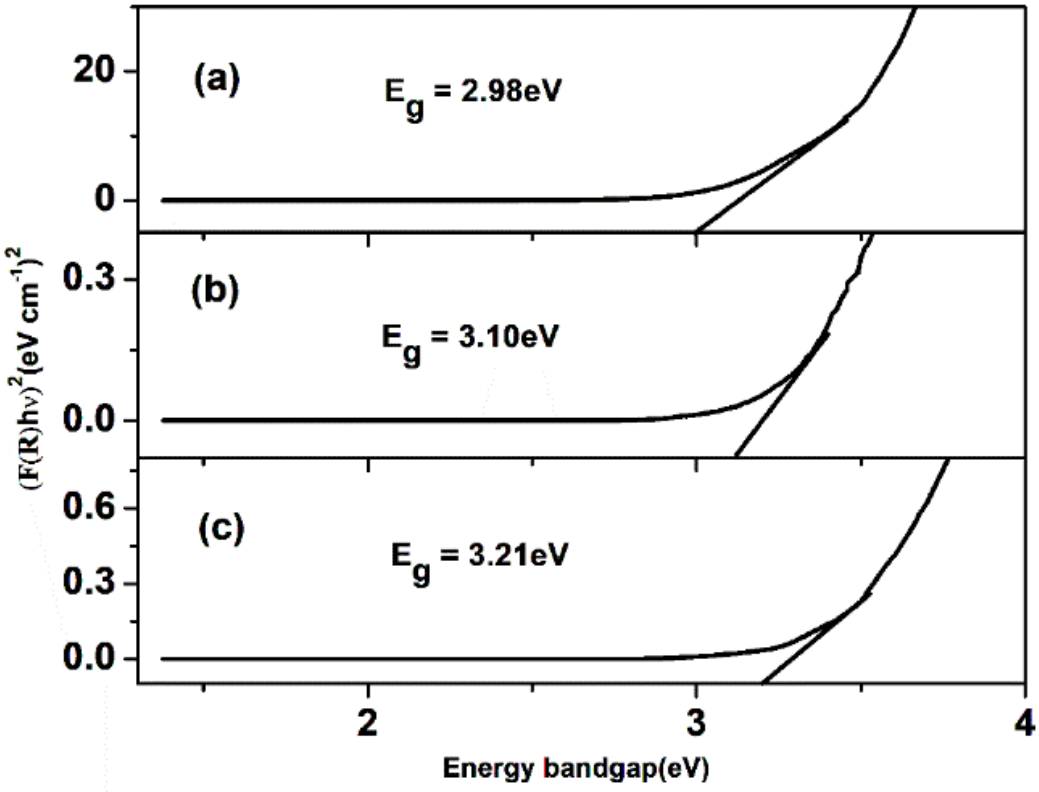

Figure 2.10: Bandgap of ITO NPs obtained using Kubelka-Munk function and photon energy with (a) ITO 5:5 (b)ITO 9:1 (c) ITO 9.5:0.5[24].

The band gap can be understood by the Burstein-Moss model which is expressed by the following Eq. 6,

$$\Delta E^{BM} = \frac{h^2}{8\pi^2 m^*}\left(3\pi^2 n\right)^{\frac{2}{3}} \quad (2.13)$$

where, m^* is the effective mass of an electron ($m^* = 0.3\ m_o$) for ITO nano-crystalline samples, $m_o$is the mass of free electron that is 9.11 x 10^{-31} kg, h is Planck's constant having a value of 6.63 x 10^{-34} J.s and n is the carrier concentration measured from Hall effect measurements[24]. The optical band gap energy calculated in this method is not the actual band gap of synthesized material. As these are degenerate semiconductors, the Fermi level recline within the CB and its position depends on the density of the free electrons. Thus, the given values of band gaps are associated to the excitation of the electrons from VB to the Fermi level in the CB, but the actual band gap of the material is because of the excitation of the electrons from top of the VB to the

bottom of the CB. This implies that the lifting of the Fermi level into the CB due to excess amount of carrier concentration leads to the energy band broadening or shiftin[21].

Table 2.3: Band gap energies of ITO.

Concentration ratio of In_2O_3 : Sn	**0.5 : 9.5**	**1 : 9**	**5 : 5**
Band gab energy (E_g) (eV)	3.21	3.10	2.98

THREE CHAPTER

3. METHODOLOGY

To do this project, the following mathematical methods will be used to study optical properties of undoped and tin doped indium oxide (In_2O_3) nano-particles.

3.1. Data Sources/ Materials

To study the optical property of undoped and tin (Sn) doped indium oxide nano-particles, a deep survey of journals and books was carried out. Data were collected from different journals and used to calculate particle size, band gap energy and index of refraction.

3.2. Mathematical Models for Determination of Band Gap Energy, crystallite Size and Index of Refraction of Undoped and Tin (Sn) Doped Indium Oxide Nano-particle

3.2.1. Deby Scherer's Equation

The average crystallite size of synthesized tin oxide nano particles is characterized by XRD. It Can be measured using Debby sheers equation as indicated in equation (3.1[19].

$$D = \frac{k\lambda}{\beta\cos(\theta)} \tag{3.1}$$

Where, D is diameter of crystallite size; k is the correction factor or constant (usually 0.9); λ is Wavelength of X-Ray source of Cu-Kα radiation (1.542Å); β is Full width at half-maximum (FWHM) of the diffraction peak in radian and θ is Bragg's diffraction angle.

It is well known that dislocation density (δ) is the measure of defects in the crystalline solids. Itis also calculated by using equation 3.2 as shown below;

$$\delta = \frac{1}{D^2} \tag{3.2}$$

Micro-strain is obtained by using equation 3.3.

$$\varepsilon = \frac{\beta \cos(\theta)}{4} \qquad \textbf{(3.3)}$$

3.2.2. Brus Model

Brus providedthe first theoretical calculations of semiconductor nano-particles (using the example of CdS and CdSet) based on the "effective mass approximation"(EMA). In this approximation, the excitons are assumed to be confined to the spherical volume of the crystallite, and the electron and hole masses are replaced by the effective masses (m_e^* and m_h^*) to define the wave function.

$$E_g\left(nanoparticle\right) - E_{bulk} = \frac{h^2}{8r^2}\left(\frac{1}{m_e^*} + \frac{1}{m_h^*}\right) \qquad \textbf{(3.4)}$$

Where, E_g = band gap energy of nanoparticle,E_{Bulk} is band gap energy of bulk semiconductor; R = radius of quantum dot; m_e^* = effective mass of excited electron; m_h^* = effective mass of excited holes; h=Planck's constant; $1.786\left(\frac{e^2}{4\pi\varepsilon_0\varepsilon_r r^2}\right)$ is columbic attraction force; ε_0 Permittivity of vacuum and ε_r is relative permittivity.

The Brus equation can be used to describe the emission energy of quantum dot semiconductor nano-crystals. The Brus equation used us to know the relation between crystallite size and wave length as well as particle size with confinement energy. The radius of the quantum dot affects the wave length of the emitted light due to quantum confinement and this describes the effect of changing radius of the quantum dot on the wavelength emitted. The effect of the surroundings will indeed probably be very small, but the effect of an externally applied potential can be quite significant. Therefore, this approximation is expected to fail when the externally applied potential becomes too large.

3.2.3. Moss Relation Formula

There are different models or formulas which are important to calculate the index of refraction of semiconductor using optical band gap energy, but in this project mainly Moss relation was used. The refractive index (n) is also an important fundamental property of tetrahedral semiconductors and it is related to the local field inside the material.

Moss proposed general relationships between refractive index (n) and optical energy gap. The Moss relation was formulated as:

$$n^4 E_g = 95 eV \tag{3.5}$$

According to Moss relation formula, the refractive index (n) of a semiconductor can be determined with a known energy gap, E_g. This relation, again, was based on the general assumption that all energy levels in a solid are scaled down by a factor of $\frac{1}{\varepsilon_{eff}^2}$, where ε_{eff} is effective dielectric constant.

Dielectric constant (k) is given by;

$$k = n^2 \tag{3.6}$$

Where k is the dielectric constant and n is the refractive index of indium oxide & ITO nanoparticles.

CHAPTER FOUR

4. RESULT AND DISCUSSION

4.1. Determination of crystallite Size of Undoped and Tin Doped Indium Oxide Nano-particle Using XRD Diffract meter

To determine the crystallitesize of pure and tin doped In_2O_3 nano-particle, the band gap energy is calculated by Deby Scherer's using experimental result gained from UV-Vis Spectroscopy analysis in review literature in table (2.1). The average crystallite size of tin doped indium oxide nano particles can be calculated and characterized by Deby Scherer's equation as indicated in equation (4.1) using XRD experimental data.

$$D = \frac{k\lambda}{\beta\cos(\theta)} \qquad (4.1)$$

Where, D is diameter of crystallite size; k is the correction factor or constant (usually 0.9); λ is Wavelength of X-Ray source of Cu-Kα radiation (1.542Å); β is Full width at half-maximum (FWHM) of the diffraction peak in radian and θ is Bragg's diffraction angle.

Table 4.1.crystallite sizes of In_2O_3nano-particle.

In_2O_3 sample at different calcined temperature (°C)	crystallite size from XRD (nm)	Cubic lattice parameter, a (nm)
450°C	12.1	1.0099
500°C	13.7	1.0092
550°C	17.1	1.0122
600°C	23.7	1.0119

We can observe from figure 4.1 that as the temperature increases, itscrystallite size is also increases.

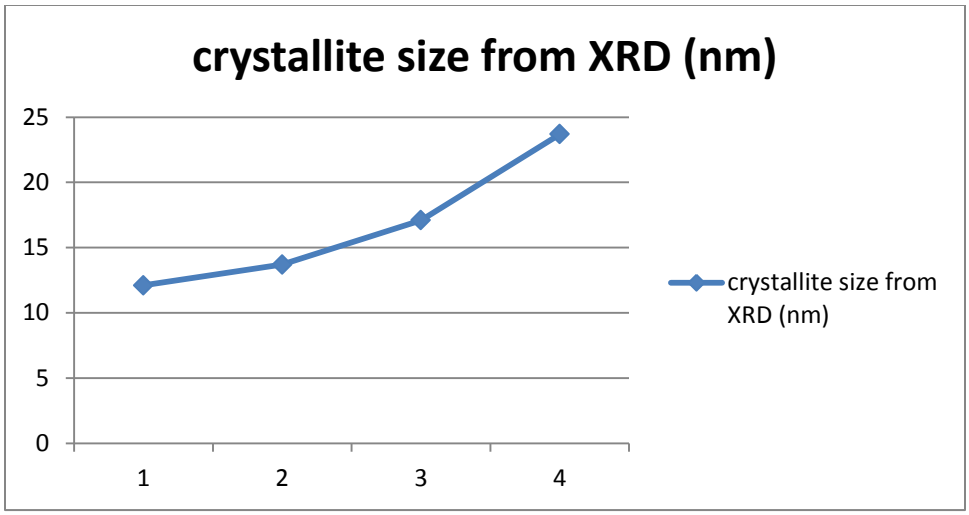

Figure 4.1: A graph of crystallite size versus temperature of indium oxide nanoparticle.

Table 4.2: crystallite sizes of tin doped In_2O_3nano-particle.

Concentration of SnO_2 In_2O_3 (%)	FWHM, β (10^{-3} radian)	λ of X-Ray source (nm)	Bragg's diffraction angle, 2θ (radian)	Estimated values ofcrystallite size, D (nm)	Calculated values ofcrystallite size, D (nm)
0.5 : 9.5	7.82	0.1542	0.5326	21.22	18.40
1 : 9	7.1	0.1542	0.5311	27.62	20.27
5 : 5	5.6	0.1542	0.5309	35.39	25.68

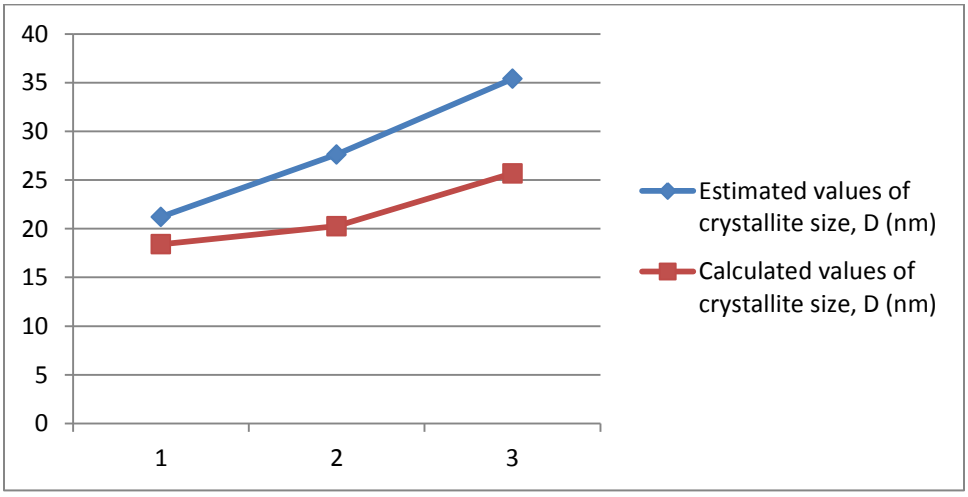

Figure 4.2: A graph of estimated and calculated values of crystallite size,D(nm)

The crystallinity of the compound increases with the increase of doping ratio from 5% to 50 %. As we can see from figure 4.2, the calculated crystallite size of ITO nano-particle is increased from 18.40 nm to 25.68 nm as Sn was added to In_2O_3. In general, there was a decrease in full width of half maximum FWHM with the increase of the doping ratio. This leads to the increase of the crystallite size as the addition of Sn in to In_2O_3 was increased.

4.2. Determination of dislocation density of undoped and tin doped indium oxide nanoparticle

The dislocation density value (δ) denotes the number of dislocation lines per unit volume ofcrystal, which is the size of the crystal defects possessed by a crystal. In other words, the dislocationdensity value will illustrate the degree of crystallinity of the nanoparticles profile. The average result of the dislocation density (δ_{np}) of the In_2O_3 nanoparticles is 4.34 x 10^{15}lines/m^2. Based on the results of this calculation,itis known that the dislocation density (δ_{np}) of the nanoparticles obtained in this study is quite small. Small dislocation density value is indicates that In_2O_3 nanoparticles have been produced had a high degree of crystallinity.

Table 4.3. Calculated values of dislocation density of In_2O_3nano-particle

In_2O_3 sample at different calcined temperature (°C)	crystallite size from XRD (nm)	Calculated values of dislocation, δ (10^{15}lines/m^2)
450°C	12.1	6.83
500°C	13.7	5.33
550°C	17.1	3.42
600°C	23.7	1.78

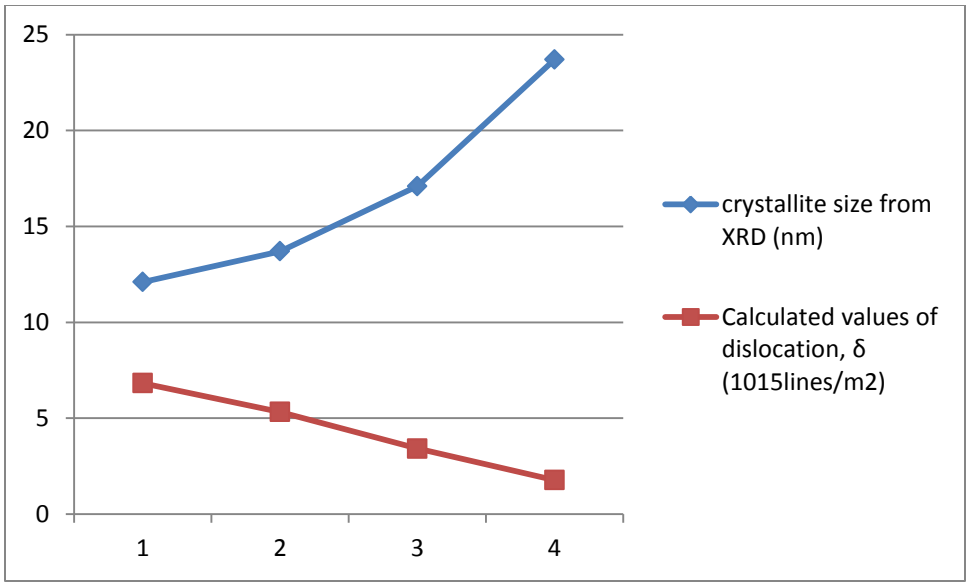

Figure 4.3: Graph of dislocation density, crystallite size and temperature of indium oxide nanoparticle.

The ITO NPs with less tin content contains spongy and more porous structures. As the Sn concentration increases stuffiness decreases. The less doped ITO NPs become less dense, with more pores and cavities. Therefore, more charge carriers are trapped in pores and cavities, which affect the conductivity of ITO NPs. According to EDAX reports, the elemental composition of synthesized ITO NPs are only In, Sn, and O, and no other impurities were observed. So, we can observe from table 4.4 that the dislocation density decreases as the concentration of tin increases.

Table 4.4: Calculated values of dislocation density of ITO nanoparticle

Concentration of SnO_2 : In_2O_3 (%)	Estimated values of crystallite size, D (nm)	Calculated values of dislocation, δ (10^{15}lines/m^2)
0.5 : 9.5	21.22	2.22
1 : 9	27.62	1.31
5 : 5	35.39	0.798

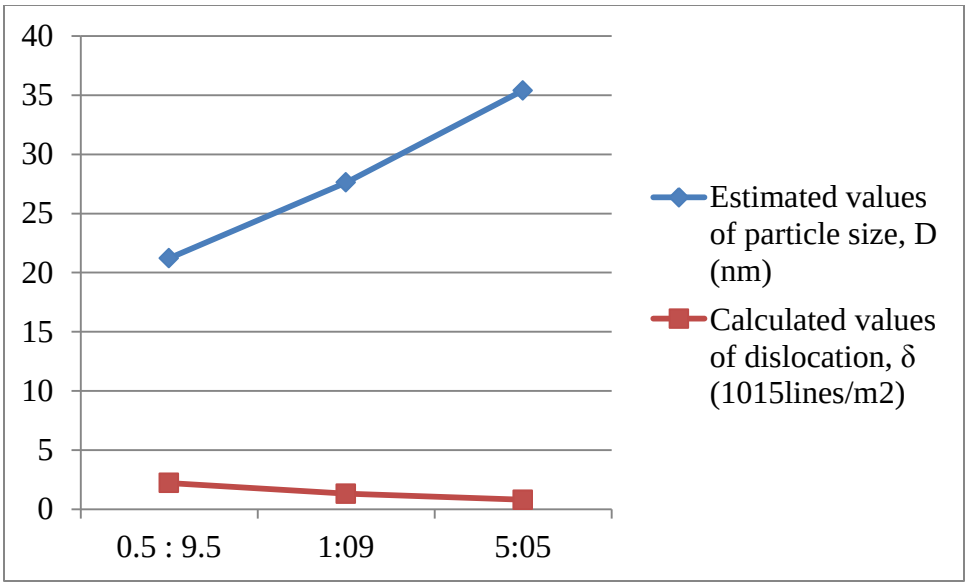

Figure 4. 4: Graph of dislocation density and particle size of ITO nanoparticle.

4.3. Determination of Micro-strain of undoped and tin doped indium oxide nanoparticle

The strain value of a crystal shows the alignment of a crystal that was produced. The crystalline strain was determined by using the diffraction pattern relationship of the line broadening that obtained in the measurement using XRD. $\beta_{h\,kl}$ is resulted by each diffraction peak of In_2O_3. The total peak broadening is the sum of the crystallite size and strain present in the material.

Theaveragemicro-strain value of nanoparticles of In_2O_3,calcined at different temperature,calculated based on the data in table 4.5 is 2223 x 10^{-6}. The value indicates that all the crystals are not far apart. In addition, this result also shows that the nanoparticle product is a lack of strain.

Table 4.5. Calculated values of micro-strain of In_2O_3nano-particle

In_2O_3 sample at different calcined temperature (°C)	crystallite size from XRD (nm)	Calculated values of micro-strain, ε (10^{-6})	Estimated values ofband gap energy, E_g (eV)
450°C	12.1	2867	3.93
500°C	13.7	2532	3.90
550°C	17.1	2029	3.70
600°C	23.7	1464	3.82

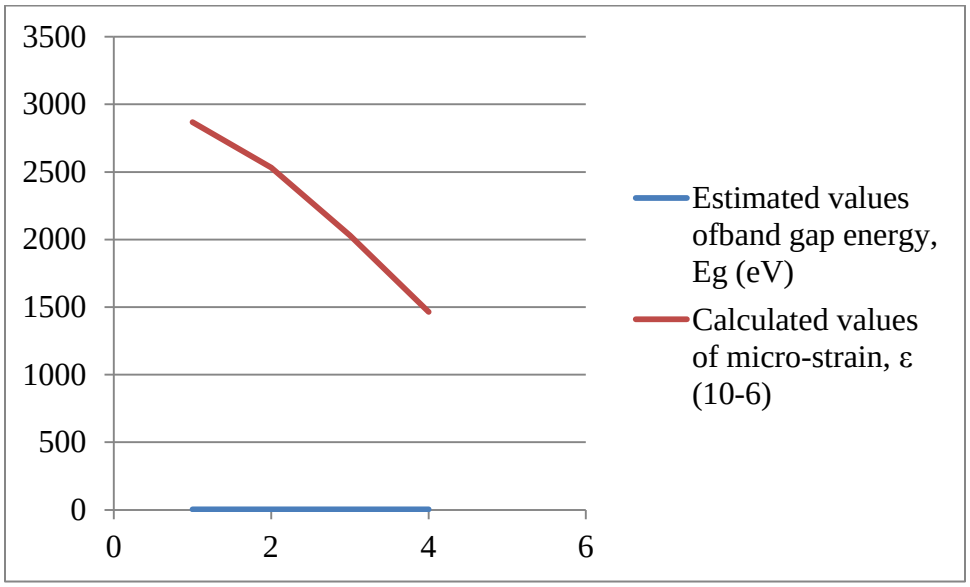

Figure 4.4: Graph of band gab energy and micro-strain of indium oxide nanoparticle

.

Table 4.6: Calculated values of micro-strain of ITO nanoparticle.

Concentration of SnO_2 : In_2O_3 (%)	FWHM, $\beta(10^{-3}$ radian)	Bragg's diffraction angle, 2θ (radian)	Estimated values ofband gap energy, E_g (eV)	Experimental values of crystallite size, D (nm)	Calculated values of micro-strain, ε (10^{-6})
0.5 : 9.5	7.82	0.5326	3.21	21.22	1954
1 : 9	7.1	0.5311	3.10	27.62	1713
5 : 5	5.6	0.5309	2.98	35.39	1351

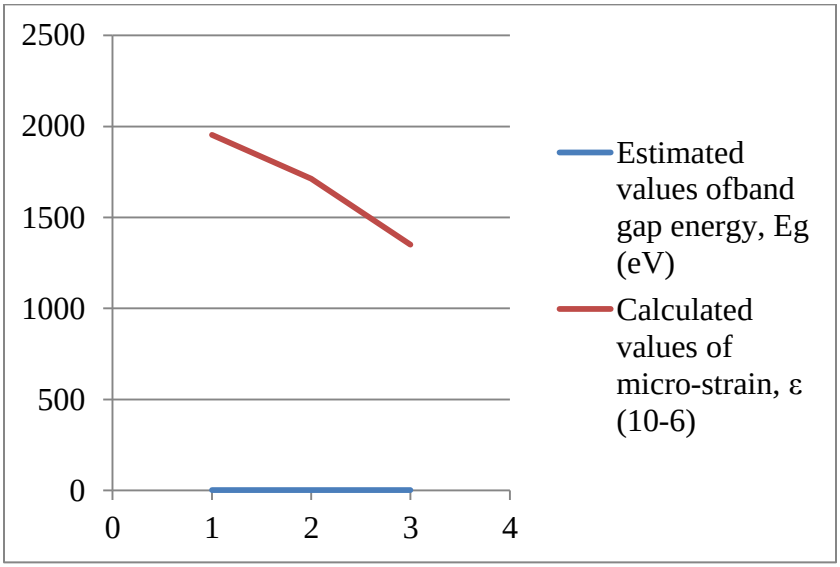

Figure 4.5: Energy gap versus calculated values of micro-strain for ITO nanoparticle.

Lattice strain decreases as the tin concentration increases because of an increase in grain size.

4.4.Determination of Band Gap Energy of Undoped and Tin (Sn) Doped Indium Oxide (In_2O_3) Nano-particle

From the experimental value of average crystallite size of tin doped indium oxide nano-particle with different concentration explained in the review literature from table 2.1 of XRD analysis, the band gap energy (E_g) in electron volt can be calculated using Brus model. The band gap of

tin doped indium oxide nano-particle using the Brus model effective mass approximation equation can be expressed as;

$$E_g\left(nanoparticle\right)-E_{bulk}=\frac{h^2}{8r^2}\left(\frac{1}{m_e^*}+\frac{1}{m_h^*}\right) \quad (4.2)$$

From equation (4.2) we have,

$$E_g\left(nanoparticle\right)-E_{bulk}=\frac{h^2}{2D^2}\left(\frac{1}{m_e^*}+\frac{1}{m_h^*}\right) \quad (4.3)$$

Where E_g (nano.) is the energy gap of nano-materials at the peak of the spectrometer, E_g (bulk) is the energy gap of bulk materials (i.e., the energy gap of a materials when no impurity is added) which is constant for the given materials (E_g(bulk)=3.7 eV for pure In_2O_3), $m_e^*=0.299m_0$, $m_h^*=0.234m_0$, but m_0 is the free electron mass which has a value of 9.11×10^{-31} kg, r is the radius of the particle size of the tin doped indium oxide and, h is the plank's constant which is equal to 6.63×10^{-34}Js. Then the particle size (D=2r is in nanometer) can also be calculated by eq. (4.3) in addition to Scherer's formula and the result of this calculated band gap energy can be expressed in the following table below.

Table 4.7. Calculated values of band gap energy of In_2O_3nano-particle.

In_2O_3 sample at different calcined temperature (°C)	crystallite size from XRD (nm)	calculatedvalues of energy band, E_g (eV)
450°C	12.1	3.78
500°C	13.7	3.76
550°C	17.1	3.74
600°C	23.7	3.72

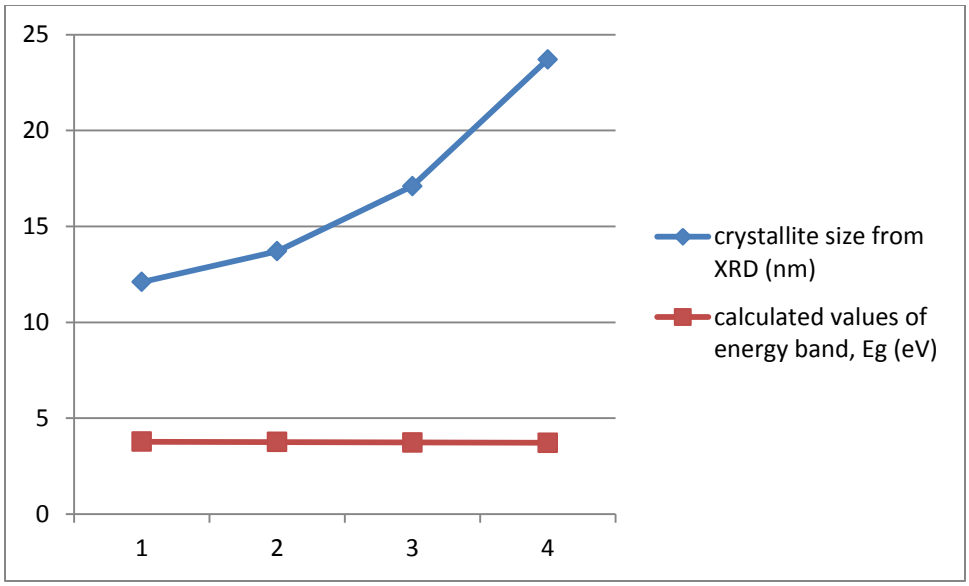

Figure 4.6: Graph of band gap energy and crystallite size versus temperature of indium oxide nanoparticle.

From the table 4.4, we can compare and contrast the particle size and band gap energy with different tin (Sn) concentration with the experimental and calculated band gap values from UV-Vis spectra. When tin (Sn)=5%, the calculated band gap energy is 3.726 eV. The experimental band gap energy values decreased as the doping concentration increases. When the tin (Sn) doped value increases, the particle size increases. This is leading to the decrease of calculated band gap energy which satisfies the mathematical relations in equation 4.3 since the particle size is inversely related to the energy gap. Therefore, the calculated band gap decreases when the Snconcentration increases like that of the experimental value which satisfies the Brus mathematical model of energy gap formula.

Table 4.8: crystallite sizes and energy band gap of tin doped In_2O_3nano-particle.

Concentration ratio of SnO_2 : In_2O_3(%)	Crystalline size,D(nm)	Calculated values of energy band gap, E_g (eV)	Estimated energy band gap, E_g (eV)
0.5 : 9.5	21.22	3.726	3.21
1 : 9	27.62	3.715	3.10
5 : 5	35.39	3.709	2.98

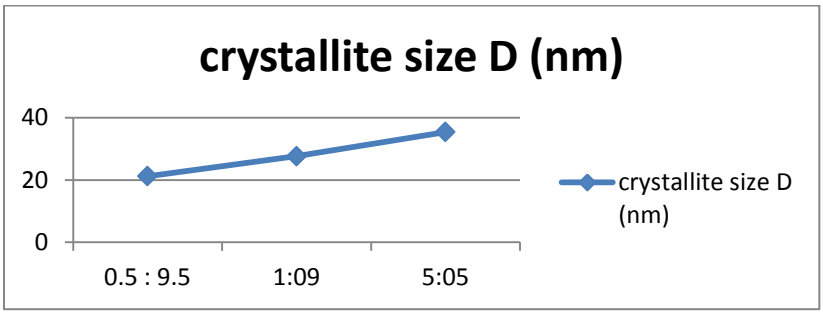

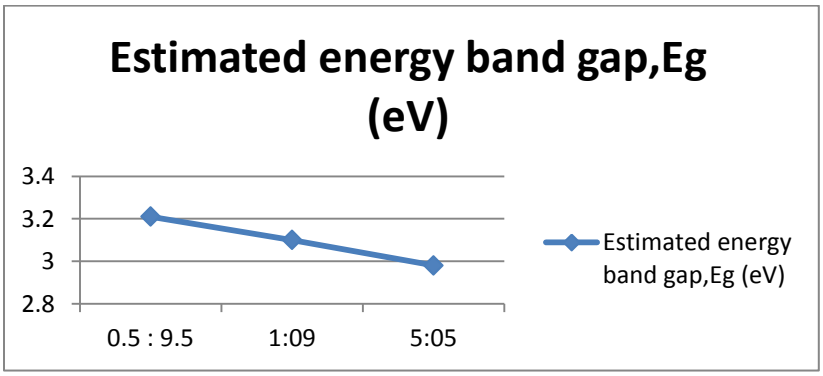

Figure 4.7: Graph of band gap energy and particle size of ITO nanoparticle

Figure 4.8: Graph of band gap energy and particle size of ITO nanoparticle.

4.5. Determination of Refractive Index (n) of Undoped and Tin (Sn) Doped Indium Oxide (In2O3) Nano-particle Using UV-Vis Spectroscopy Spectra

The refractive index can be calculated using Moss relation formula as given in equation (4.6). Indeed n increases from 2.33 to 2.38 with the increase of doping ratio from 5% to 50% tin. The increase of the refractive index (n) attributed to the reduction of transmittance giving rise to high opaque material while the reduction of the refractive index (n) is related to the inverse manner. The values of refractive index are given in table 4.3. From equation (3.5) of Moss relation with band gap formula, Refractive index is expressed as;

$$n^4 E_g = 95eV \tag{4.4}$$

Where E_g is the calculated energy band gap of tin doped In_2O_3nano-particle. Thus, we get;

$$n^4 = \frac{95eV}{E_g} \tag{4.5}$$

$$n = \left(\frac{95eV}{E_g}\right)^{\frac{1}{4}} \tag{4.6}$$

Using these relations, the calculated index of refraction of tin doped indium oxide nano-particle can be expressed in the following table below.

Table 4.9: Calculated values of refractive index of In_2O_3nano-particle.

In_2O_3 sample at different calcined temperature (°C)	Estimated Energy band gap, E_g (eV)	Calculated values of refractive index, n
450°C	3.93	2.217
500°C	3.90	2.222
550°C	3.70	2.251
600°C	3.82	2.233

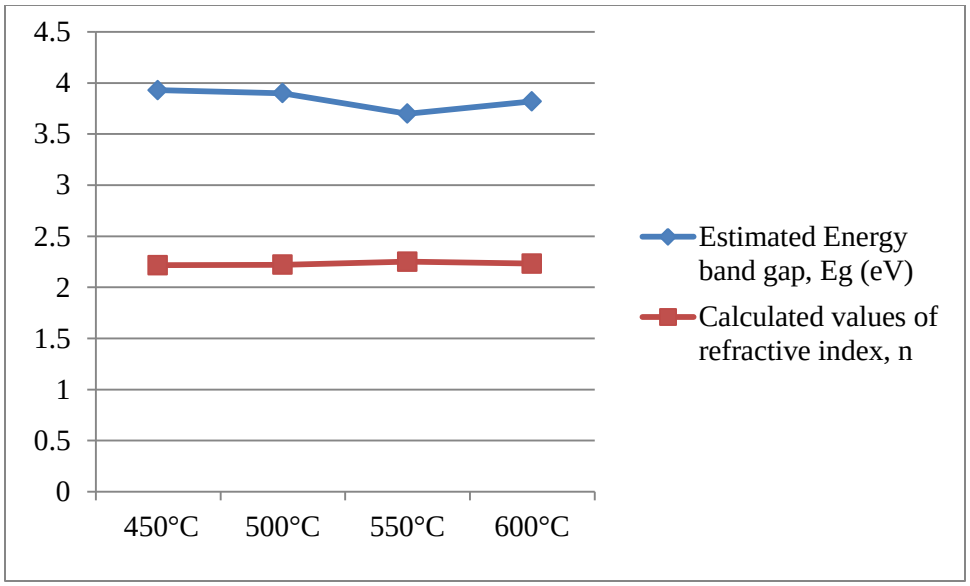

Figure 4.9: Graph of band gap, refractive index versus temperature of indium oxide nanoparticle

Table 4.10: Band gap energy and index of refraction of tin doped In_2O_3nano-particle

Concentration ratio of $SnO_2 : In_2O_3$(%)	Estimated values ofband gap energy, E_g (eV)	Calculated values of refraction index, n
0.5 : 9.5	3.21	2.33
1 : 9	3.10	2.35
5 : 5	2.98	2.38

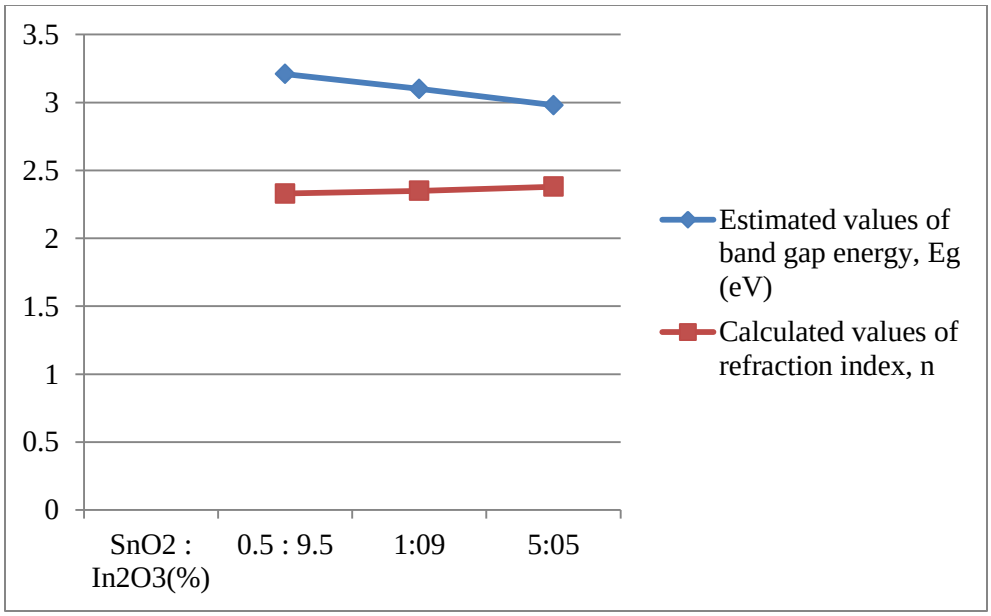

Figure 4.10: Graph of refractive index and band gap of ITO nanoparticle.

From figure 4.2, we can conclude that refractive index increases with the decrease in band gap, but with increasing of concentration. Conductivity increases due to the release of the electron by substituting donor Sn^{4+} ion for In^{3+} ion in In_2O_3 as Sn concentration increases, which induces an extra electron into the conduction band and carrier density increases. Hence ITO 5:5 has more conductivity as compared to sample ITO 9:1 and ITO 9.5:0.5 as shown in figure 4.3.

4.6. Determination of dielectric constant of undoped and tin doped indium oxide nanoparticle

The dielectric constant of a material provides a measure of its effect on a capacitor. It is the ratio of the capacitance of a capacitor containing the dielectric to that of an identical but empty capacitor.An alternative definition of the dielectric constant relates to the permittivity of the material. Permittivity is a quantity that describes the effect of a material on an electric field: the higher the permittivity, the more the material tends to reduce any field set up in it. Since the dielectric material reduces the field by becoming polarized, an entirely equivalent definition is that the permittivity expresses the ability of a material to polarize in response to an applied field. The dielectric constant (sometimes called the 'relative permittivity') is the ratio of the permittivity of the dielectric to the permittivity of a vacuum, so the greater the polarization developed by a material in an applied field of given strength, the greater the dielectric constant will be. There is no standard symbol for the dielectric constant – you may see it referred to as k, ε, ε' or ε_r. In this project, k shall be used to avoid confusion.

In general, the more available polarization mechanisms a material possesses, the larger its net polarization in a given field will be and hence the larger its dielectric constant will be.The dielectric constant of a material and its refractive index are closely linked by the equation $k = n^2$. However, care must be taken in applying this equation. It is only strictly accurate when the dielectric constant and the refractive index are measured under the same conditions. Specifically, since the dielectric constant can vary significantly with frequency, we must measure the dielectric constant under alternating current at the same frequency that we measure the refractive index at – the frequency of visible light, ~10^{15} Hz. However, quoted values of the dielectric constant normally refer to the static dielectric constant – that is, the dielectric constant under direct current. This is often very different from the value of the dielectric constant at 10^{15} Hz.

The exception to this is for materials that possess only the electronic mode of polarization. For these materials, the dielectric constant does not vary significantly with frequency below visible frequencies, and $k_S \approx n^2$ where $k_S$are the static dielectric constant. So the equation $k = n^2$ can be applied to the static dielectric constants of non-polar materials only, or to the high-frequency dielectric constants of any dielectric.

Table 4.11: Calculated values of dielectric constant of In_2O_3 nanoparticle

In_2O_3 sample at different calcined temperature (°C)	Dielectric constant, ε	Refractive index, n	Estimated Energy band gap, E_g (eV)
450°C	4.915	2.217	3.93
500°C	4.937	2.222	3.90
550°C	5.067	2.251	3.70
600°C	4.986	2.233	3.82

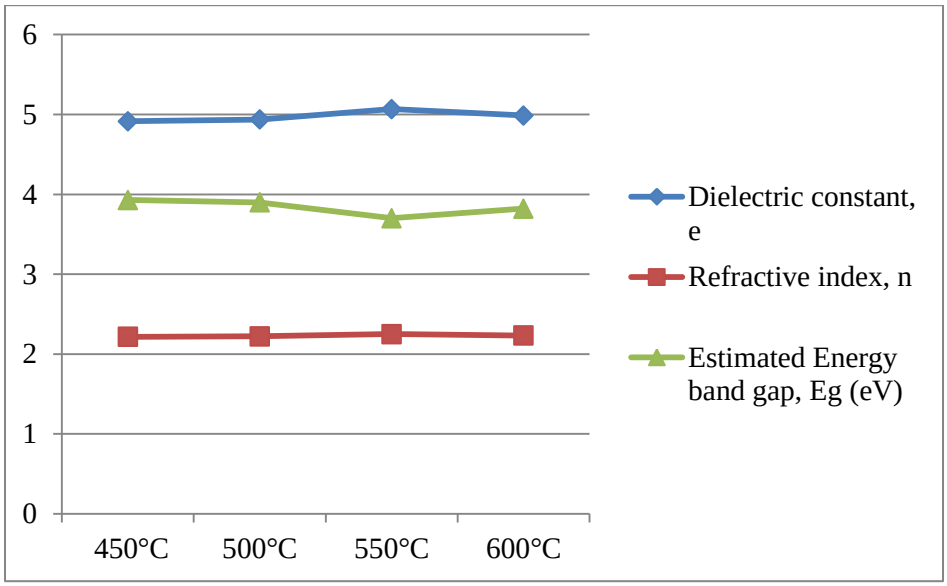

Figure 4.11: Graph of band gap, refractive index and dielectric constant of indium oxide nanoparticle.

The dielectric medium is assumed to be composed of double layers, conductive grains, and resistive grain boundaries. Upon the application of electric field, charge carriers can easily move from grains but are collected at grain boundaries. This process can create large polarization and dielectric constant. As frequency increases, the dielectric constant decreases because of the ability of dipoles to orient them to the applied electric field. In the high-frequency region (above 1000 Hz), the dipoles will be strongly oriented to an applied field. Hence dielectric constant for ITO NPs becomes constant at the high-frequency region. Grain boundary resistance decreases as tin concentration increases, which is useful for the improvement of electrical conductivity.

Table 4.12: Calculated values of dielectric constant of tin doped In_2O_3 nanoparticle

Concentration of SnO_2 : In_2O_3 (%)	Estimated values of band gap energy, E_g (eV)	Calculated values dielectric constant	Calculated values of refraction index, n
0.5 : 9.5	3.21	5.43	2.33
1 : 9	3.10	5.52	2.35
5 : 5	2.98	5.66	2.38

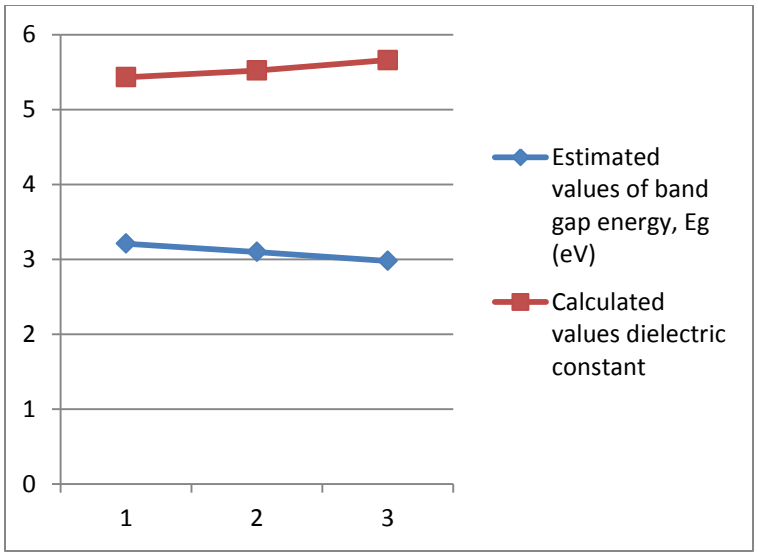

Figure 4.12: Graph of band gap energy and dielectric constant of ITO nanoparticle.

CHAPTER FIVE

5. CONCLUSIONS

In this project work, the energy band gap , particle size and index of refraction of undoped and tin doped In_2O_3nano-particle was calculated based on XRD, UV-Vis and photoluminescence spectroscopic data using Brus equations, Deby Scherer's formula and Moss relation formula. From the experimental data, the energy band gap is decreased and the particles size increased as the tin concentration increased. When the tin concentration increases from 5% to 50 %, the calculated particle size increases from 18.40 nm to 25.68 nm, but the calculated energy band gap decreases from 3.726 eV to 3.709 eV. Therefore, both the calculated and experimental values of the particle size of XRD analysis is increased when the tin percent in the sample is increased. The calculated band gap energy of ITO nanoparticle is decreased by increasing the tin concentration like that of the experimental value of band gap energy which is decreased as the tin concentration increases. The calculated index of refraction of tin doped indium oxide nanoparticle increases from 2.33 to 2.38 as tin concentration increases which is attributed to the reduction of transmittance giving rise to high opaque material while the reduction of the refractive index (n) is related to the inverse manner.

Generally in this project work, it is possible to conclude that when we add an impurity of tin in to pure indium oxide there is a change in structure and optical properties of ITO nano-particle, which means there is a change in particle size, band gap energy and index of refraction. Therefore, for different types of impurity added to the semiconductor, there is a different optical property of the semiconductor. The crystallite size of the nano-particle was calculated using Debye-Scherer formula which varies from 18.40 – 25.68 nm. The calculated band gap energies decrease if the Sn concentration increases, as a result of the occurrence of additional energetic levels in the forbidden gap. Optical analysis of UV-Vis indicates that the increasing of tin concentration made all the prepared nano-particles more opaque throughout increasing the packing density and shifting the absorption edge to lower energies. Increasing of tin oxide content in the prepared samples creates new states in the band gap which consequently giving rise to the visual decrease of the optical energy gap.

References

[1] C. A. Buckner et al., “We are IntechOpen , the world ’ s leading publisher of Open Access books Built by scientists , for scientists TOP 1 %,” Intech, vol. 11, no. tourism, p. 13, 2016, [Online]. Available: https://www.intechopen.com/books/advanced-biometric-technologies/liveness-detection-in-biometrics

[2] A. Fattahi, P. Koohsari, M. S. Lakmehsari, and K. Ghandi, “The Impact of the Surface Modification on Tin-Doped Indium Oxide Nanocomposite Properties,” Nanomaterials, vol. 12, no. 1, 2022, doi: 10.3390/nano12010155.

[3] J. Kim, S. Shrestha, M. Souri, J. G. Connell, S. Park, and A. Seo, “High-temperature optical properties of indium tin oxide thin-films,” Sci. Rep., vol. 10, no. 1, pp. 1–8, 2020, doi: 10.1038/s41598-020-69463-4.

[4] E. A. Forsh et al., “Optical and photoelectrical properties of nanocrystalline indium oxide with small grains,” Thin Solid Films, vol. 595, no. October, pp. 25–31, 2015, doi: 10.1016/j.tsf.2015.10.053.

[5] O. Bierwagen, “Indium oxide - A transparent, wide-band gap semiconductor for (opto)electronic applications,” Semicond. Sci. Technol., vol. 30, no. 2, p. 24001, 2015, doi: 10.1088/0268-1242/30/2/024001.

[6] S. Cao et al., “3D Porous Pyramid Heterostructure Array Realizing Efficient Photo-Electrochemical Performance,” Adv. Energy Mater., vol. 10, no. 5, pp. 1–9, 2020, doi: 10.1002/aenm.201902935.

[7] N. Dilawar, S. Mehrotra, D. Varandani, B. V. Kumaraswamy, S. K. Haldar, and A. K. Bandyopadhyay, “A Raman spectroscopic study of C-type rare earth sesquioxides,” Mater. Charact., vol. 59, no. 4, pp. 462–467, 2008, doi: 10.1016/j.matchar.2007.04.008.

[8] S. Bera, A. Haldar, M. Pal, S. Sarkar, R. Chakraborty, and S. Jana, “Zinc-indium-oxide sol-gel thin film: Surface patterning, morphology and photocatalytic activity,” Surf. Eng., vol. 31, no. 7, pp. 492–501, 2015, doi: 10.1179/1743294414Y.0000000414.

[9] P. Li and H. Fan, “Porous in2O3 microstructures: Hydrothermal synthesis and enhanced Cl2 sensing performance,” Mater. Sci. Semicond. Process., vol. 29, pp. 83–89, 2015, doi: 10.1016/j.mssp.2013.09.026.

[10] S. Sundaresh, S. D. Nehate, and K. B. Sundaram, “Electrical and Optical Studies of

Reactively Sputtered Indium Oxide Thin Films," ECS J. Solid State Sci. Technol., vol. 10, no. 6, p. 065016, 2021, doi: 10.1149/2162-8777/ac0a51.

[11] Y. K. Lv, Y. Y. Li, R. H. Zhou, Y. P. Pan, H. C. Yao, and Z. J. Li, "N-Doped Graphene Quantum Dot-Decorated Three-Dimensional Ordered Macroporous In2O3for NO2Sensing at Low Temperatures," ACS Appl. Mater. Interfaces, vol. 12, no. 30, pp. 34245–34253, 2020, doi: 10.1021/acsami.0c03369.

[12] S. Jana and P. K. Biswas, "Effect of Zr (IV) doping on the optical properties of sol-gel based nanostructured indium oxide films on glass," Mater. Chem. Phys., vol. 117, no. 2–3, pp. 511–516, 2009, doi: 10.1016/j.matchemphys.2009.06.038.

[13] R. Geiger, T. Zabel, and H. Sigg, "Group IV direct band gap photonics: Methods, challenges, and opportunities," Front. Mater., vol. 2, no. July, 2015, doi: 10.3389/fmats.2015.00052.

[14] M. Marezio, " Refinement of the crystal structure of In 2 O 3 at two wavelengths ," Acta Crystallogr., vol. 20, no. 6, pp. 723–728, 1966, doi: 10.1107/s0365110x66001749.

[15] A. Walsh et al., "Nature of the band gap of In2O3 revealed by first-principles calculations and X-ray spectroscopy," Phys. Rev. Lett., vol. 100, no. 16, 2008, doi: 10.1103/PhysRevLett.100.167402.

[16] V. Mursyalaat, V. I. Variani, W. O. S. Arsyad, and M. Z. Firihu, "The development of program for calculating the band gap energy of semiconductor material based on UV-Vis spectrum using delphi 7.0," J. Phys. Conf. Ser., vol. 2498, no. 1, pp. 0–5, 2023, doi: 10.1088/1742-6596/2498/1/012042.

[17] R. D. Shannon, "Revised effective ionic radii and systematic studies of interatomic distances in halides and chalcogenides," Acta Crystallogr. Sect. A, vol. 32, no. 5, pp. 751–767, 1976, doi: 10.1107/S0567739476001551.

[18] S. Manafi, S. Tazikeh, and S. Joughehdoust, "Synthesis and characterization of indium tin oxide nanoparticles via reflux method," Mater. Sci. Pol., vol. 35, no. 4, pp. 799–805, 2017, doi: 10.1515/msp-2018-0008.

[19] S. Sonsupap, E. Swatsitang, S. Maensiri, and K. Wongsaprom, "Synthesis and characterization of indium oxide nanoparticles using indium nitrate and polyvinylpyrrolidone W(PVP) as precursors," Chiang Mai J. Sci., vol. 42, no. 3, pp. 752–760, 2015.

[20] S. Sonsupap and K. Wongsaprom, “Synthesis and Characterization of Indium Oxide Nanoparticles Using Indium Nitrate and Polyvinylpyrrolidone (PVP) as Precursors,” vol. 42, no. 3, pp. 752–760, 2015.

[21] S. Z. Karazhanov, P. Ravindran, P. Vajeeston, A. Ulyashin, T. G. Finstad, and H. Fjellvåg, “Phase stability, electronic structure, and optical properties of indium oxide polytypes,” Phys. Rev. B - Condens. Matter Mater. Phys., vol. 76, no. 7, pp. 1–13, 2007, doi: 10.1103/PhysRevB.76.075129.

[22] Z. Ma, Z. Li, B. M. Nouri, K. Liu, C. Ye, and H. Dalir, “Indium-Tin-Oxide for High-performance Electro-optic Modulation,” pp. 1–36.

[23] M. Seetha, S. Bharathi, A. Dhayal Raj, D. Mangalaraj, and D. Nataraj, “Optical investigations on indium oxide nano-particles prepared through precipitation method,” Mater. Charact., vol. 60, no. 12, pp. 1578–1582, 2009, doi: 10.1016/j.matchar.2009.09.009.

[24] J. Ederth et al., “Electrical and optical properties of thin films consisting of tin-doped indium oxide nanoparticles,” Phys. Rev. B - Condens. Matter Mater. Phys., vol. 68, no. 15, 2003, doi: 10.1103/PhysRevB.68.155410.

[25] V. Gowthami, M. Meenakshi, N. Anandhan, and C. Sanjeeviraja, “Structural and optical properties of nebulized nickel oxide thin films,” Adv. Mater. Res., vol. 938, no. 1, pp. 103–107, 2014, doi: 10.4028/www.scientific.net/AMR.938.103.

[26] V. Kachkanov et al., “Structural dynamics of GaN microcrystals in evolutionary selection selective area growth probed by X-ray microdiffraction,” Sci. Rep., vol. 4, pp. 4–9, 2014, doi: 10.1038/srep04651.

[27] A. H. Sofi, M. A. Shah, and K. Asokan, “Structural, Optical and Electrical Properties of ITO Thin Films,” J. Electron. Mater., vol. 47, no. 2, pp. 1344–1352, 2018, doi: 10.1007/s11664-017-5915-9.

APPENDIX 1

Calculation of Crystallite Size (D) of In_2O_3 Nano-particle

The crystallite size of ITO can be calculated by;

$$D = \frac{k\lambda}{\beta \cos\theta}$$

Where D is the crystallite size, k is the correction factor which has a value of 0.9, λ is the wave length of incident light (i.e. λ = 1.542 $\overset{0}{A}$), β is the FWHM given in radian and θ is diffraction angle of the light.

$$D_1 = \frac{\kappa\lambda}{\beta_1 \cos(\theta_1)} = \frac{0.9 \times 0.1542\,nm}{0.01146942149} \approx 12.1nm$$

$$D_2 = \frac{\kappa\lambda}{\beta_2 \cos(\theta_2)} = \frac{0.9 \times 0.1542\,nm}{0.01012992701} \approx 13.7\,nm$$

$$D_3 = \frac{\kappa\lambda}{\beta_3 \cos(\theta_3)} = \frac{0.9 \times 0.1542\,nm}{0.00811578947} \approx 17.1nm$$

$$D_4 = \frac{\kappa\lambda}{\beta_4 \cos(\theta_4)} = \frac{0.9 \times 0.1542\,nm}{0.0058556962} \approx 23.7\,nm$$

$$D_{Average} = \frac{D_1 + D_2 + D_3 + D_4}{4} = \frac{12.1nm + 13.7nm + 17.1nm + 23.7nm}{4} = \frac{66.6\,nm}{4} \approx 16.65\,nm$$

Calculation of Dislocation Density (δ) of In_2O_3 Nano-particle

Dislocation density (δ) is given by;

$$\delta = \frac{1}{D^2}$$

$$\delta_1 = \frac{1}{D_1^2} = \frac{1}{(12.1\text{nm})^2} = 6.83 \times \frac{10^{15}}{m^2}$$

$$\delta_2 = \frac{1}{D_2^2} = \frac{1}{(13.7\text{nm})^2} = 5.33 \times \frac{10^{15}}{m^2}$$

$$\delta_3 = \frac{1}{D_3^2} = \frac{1}{(17.1\text{nm})^2} = 3.42 \times \frac{10^{15}}{m^2}$$

$$\delta_4 = \frac{1}{D_4^2} = \frac{1}{(23.7\text{nm})^2} = 1.78 \times \frac{10^{15}}{m^2}$$

$$\delta_{Average} = \frac{\delta_1 + \delta_2 + \delta_3 + \delta_4}{4} = \frac{(6.83+5.33+3.42+1.78)\times 10^{15}/m^2}{4} = \frac{17.36\times 10^{15}/m^2}{4} \approx 4.34\times 10^{15}/m^2$$

Calculation of Micro-strain (ε) of In_2O_3 Nano-particle

Micro-strain (ε) is given by;

$$\varepsilon_1 = \frac{\beta_1 \cos\theta_1}{4} = \frac{0.01146942149}{4} \approx 2867 \times 10^{-6}$$

$$\varepsilon_2 = \frac{\beta_2 \cos\theta_2}{4} = \frac{0.01012992701}{4} \approx 2532 \times 10^{-6}$$

$$\varepsilon_3 = \frac{\beta_3 \cos\theta_3}{4} = \frac{0.00811578947}{4} \approx 2029 \times 10^{-6}$$

$$\varepsilon_4 = \frac{\beta_4 \cos\theta_4}{4} = \frac{0.0058556962}{4} \approx 1464 \times 10^{-6}$$

$$\varepsilon_{Average} = \frac{\varepsilon_1 + \varepsilon_2 + \varepsilon_3 + \varepsilon_4}{4} = \frac{(2867+2532+2029+1464)\times 10^{-6}}{4} = \frac{8892\times 10^{-6}}{4} \approx 2223\times 10^{-6}$$

Calculation of Band Gap Energies (E_g) of In_2O_3 Nano-particle

$$E_g(nano) = E_g(bulk) + \frac{h^2}{2D^2}\left[\frac{1}{m_e^*} + \frac{1}{m_h^*}\right]$$

$$Where, E_g(Bulk) = 3.7\,eV, m_e^* = 0.299m_0, m_h^* = 0.234m_0, m_0 = 9.11\times 10^{-31}\,kg \text{ and } h = 6.63\times 10^{-34}\,Js$$

$$E_g(nano) = 3.7\,eV + \frac{(6.63\times 10^{-34}\,Js)^2}{2(D)^2}\left[\frac{1}{0.299m_0} + \frac{1}{0.234m_0}\right] = 3.7\,eV + \frac{43.9569\times 10^{-68}\,J^2s^2}{2(D)^2}\left[\frac{0.234+0.299}{0.63739026\times 10^{-31}\,kg}\right]$$

$$E_g = 3.7eV + \frac{11.49\times 10^{-18}\,eVm^2}{D^2}$$

$$E_1 = 3.7eV + \frac{11.49\times 10^{-18}\,eVm^2}{D_1^2} = 3.7\,eV + \frac{11.49\times 10^{-18}\,eV\,m^2}{(12.1nm)^2} \approx 3.78\,eV$$

$$E_2 = 3.7eV + \frac{11.49\times 10^{-18}\,eVm^2}{D_2^2} = 3.7\,eV + \frac{11.49\times 10^{-18}\,eV\,m^2}{(13.7\,nm)^2} \approx 3.76\,eV$$

$$E_3 = 3.7eV + \frac{11.49\times10^{-18}\,eVm^2}{D_3^2} = 3.7\,eV + \frac{11.49\times10^{-18}\,eV\,m^2}{(17.1nm)^2} \approx 3.74\,eV$$

$$E_4 = 3.7eV + \frac{11.49\times10^{-18}\,eVm^2}{D_4^2} = 3.7\,eV + \frac{11.49\times10^{-18}\,eV\,m^2}{(23.7\,nm)^2} \approx 3.72\,eV$$

$$E_{g,\,Average} = \frac{E_1 + E_2 + E_3 + E_4}{4} = \frac{3.78eV + 3.76eV + 3.74eV + 3.72eV}{4} = \frac{15eV}{4} \approx 3.75eV$$

Calculation of Index of Refraction (n) of In_2O_3 Nano-particle

Index of refraction of In_2O_3 is given by;

$$n^4 E_g = 95eV \Rightarrow n^4 = \frac{95eV}{E_g} \Rightarrow n = \left(\frac{95eV}{E_g}\right)^{\frac{1}{4}}$$

$$n_1 = \left(\frac{95eV}{E_1}\right)^{\frac{1}{4}} = \left(\frac{95eV}{3.93eV}\right)^{\frac{1}{4}} = 2.217$$

$$n_2 = \left(\frac{95eV}{E_2}\right)^{\frac{1}{4}} = \left(\frac{95eV}{3.90eV}\right)^{\frac{1}{4}} = 2.222$$

$$n_3 = \left(\frac{95eV}{E_3}\right)^{\frac{1}{4}} = \left(\frac{95eV}{3.70eV}\right)^{\frac{1}{4}} = 2.251$$

$$n_4 = \left(\frac{95eV}{E_4}\right)^{\frac{1}{4}} = \left(\frac{95eV}{3.82eV}\right)^{\frac{1}{4}} = 2.233$$

$$n_{Average} = \frac{n_1 + n_2 + n_3 + n_4}{4} = \frac{2.217 + 2.221 + 2.251 + 2.233}{4} = \frac{8.922}{4} \approx 2.231$$

Calculation of Dielectric Constant (k) of In_2O_3 Nano-particle

Dielectric Constant (k) is given by;

$$k = n^2$$

$$k_1 = n_1^2 = (2.217)^2 = 4.915089 \approx 4.92$$

$$k_2 = n_2^2 = (2.222)^2 = 4.937284 \approx 4.94$$

$$k_3 = n_3^2 = (2.251)^2 = 5.067001 \approx 5.07$$

$$k_4 = n_4^2 = (2.233)^2 = 4.986289 \approx 4.99$$

$$k_{Average} = \frac{k_1 + k_2 + k_3 + k_4}{4} = \frac{4.92 + 4.94 + 5.07 + 4.99}{4} = \frac{19.92}{4} \approx 4.98$$

APPENDIX 2

Calculation of Crystallite Size (D) of ITO Nano-particle

The crystallite size of ITO can be calculated by;

$$D = \frac{k\lambda}{\beta \cos\theta}$$

Where D is the crystallite size, k is the correction factor which has a value of 0.9, λ is the wave length of incident light (i.e. λ = 1.542 $\overset{0}{A}$), β is the FWHM given in radian and θ is diffraction angle of the light.

$$D_1 = \frac{k\lambda}{\beta_1 \cos\theta} = \frac{0.9 \times 0.1542\,nm}{0.00782 \times \cos(15.26^\circ)} = \frac{0.13878\,nm}{0.00782 \times 0.96474140} = 18.40\,nm$$

$$D_2 = \frac{k\lambda}{\beta_2 \cos\theta} = \frac{0.9 \times 0.1542\,nm}{0.00710 \times \cos(15.215^\circ)} = \frac{0.13878\,nm}{0.00710 \times 0.96494782} = 20.26\,nm$$

$$D_3 = \frac{k\lambda}{\beta_3 \cos\theta} = \frac{0.9 \times 0.1542}{0.00560 \times \cos(15.2^\circ)} = \frac{0.13710984\,nm}{0.00560 \times 0.965016} = 25.68\,nm$$

$$D_{Average} = \frac{D_1 + D_2 + D_3}{3} = \frac{18.40nm + 20.26nm + 25.68nm}{3} = \frac{64.34nm}{3} \approx 21.45nm$$

Calculation of Dislocation Density (δ)of ITO Nano-particle

Dislocation density (δ) is given by;

$$\delta = \frac{1}{D^2}$$

$$\delta_1 = \frac{1}{D_1^2} = \frac{1}{(21.22\text{nm})^2} = 2.22 \times \frac{10^{15}}{m^2}$$

$$\delta_2 = \frac{1}{D_2^2} = \frac{1}{(27.62\text{nm})^2} = 1.31 \times \frac{10^{15}}{m^2}$$

$$\delta_3 = \frac{1}{D_3^2} = \frac{1}{(35.39\text{nm})^2} = 0.798 \times \frac{10^{15}}{m^2}$$

$$\delta_{Average} = \frac{\delta_1 + \delta_2 + \delta_3}{3} = \frac{(2.22+1.31+0.798)\times 10^{15}/m^2}{3} = \frac{4.328\times 10^{15}/m^2}{3} \approx 1.44\times 10^{15}/m^2$$

Calculation of Micro-strain(ε) of ITO Nano-particle

Micro-strain (ε) is given by;

$$\varepsilon_1 = \frac{\beta_1 \cos\theta_1}{4} = \frac{7.82 \times 10^{-3} \times \cos\left(\frac{30.52}{2}\right)}{4} \approx 1954 \times 10^{-6}$$

$$\varepsilon_2 = \frac{\beta_2 \cos\theta_2}{4} = \frac{7.10 \times 10^{-3} \times \cos\left(\frac{30.43}{2}\right)}{4} \approx 1713 \times 10^{-6}$$

$$\varepsilon_3 = \frac{\beta_3 \cos\theta_3}{4} = \frac{5.60 \times 10^{-3} \times \cos\left(\frac{30.42}{2}\right)}{4} \approx 1351 \times 10^{-6}$$

$$\varepsilon_{Average} = \frac{\varepsilon_1 + \varepsilon_2 + \varepsilon_3}{3} = \frac{(1954+1713+1351)\times 10^{-6}}{3} = \frac{5018\times 10^{-6}}{3} \approx 1673\times 10^{-6}$$

Calculation of Band Gap Energies (E_g) of ITO Nano-particle

$$E_g(nano) = E_g(Bulk) + \frac{h^2}{2D^2}\left[\frac{1}{m_e^*} + \frac{1}{m_h^*}\right],$$

$$Where, E_g(Bulk) = 3.7\,eV, m_e^* = 0.299m_0, m_h^* = 0.234m_0, m_0 = 9.11\times 10^{-31}\,kg \text{ and } h = 6.63\times 10^{-34}\,Js$$

$$E_g(nano) = 3.7\,eV + \frac{(6.63\times 10^{-34}\,Js)^2}{2(D)^2}\left[\frac{1}{0.299m_0} + \frac{1}{0.234m_0}\right] = 3.7\,eV + \frac{43.9569\times 10^{-68}\,J^2s^2}{2(D)^2}\left[\frac{0.234+0.299}{0.63739026\times 10^{-31}\,kg}\right]$$

$$E_g = 3.7\,eV + \frac{11.49\times10^{-18}\,eV\,m^2}{D^2}$$

$$E_1 = 3.7\,eV + \frac{11.49\times10^{-18}\,eV\,m^2}{(D_1)^2} = 3.7\,eV + \frac{11.49\times10^{-18}\,eV\,m^2}{(21.22\times10^{-9}\,m)^2}$$

$$E_1 = 3.7\,eV + \frac{11.49\times10^{-18}\,eV\,m^2}{450.2884\times10^{-18}\,m^2} = 3.7\,eV + 0.026\,eV \approx 3.726\,eV$$

$$E_2 = 3.7\,eV + \frac{11.49\times10^{-18}\,eV\,m^2}{(D_2)^2} = 3.7\,eV + \frac{11.49\times10^{-18}\,eV\,m^2}{(27.62\times10^{-9}\,m)^2}$$

$$E_2 = 3.7\,eV + \frac{11.49\times10^{-18}\,eV\,m^2}{762.8644\times10^{-18}\,m^2} = 3.7\,eV + 0.015\,eV \approx 3.715\,eV$$

$$E_3 = 3.7\,eV + \frac{11.49\times10^{-18}\,eV\,m^2}{(D_3)^2} = 3.7\,eV + \frac{11.49\times10^{-18}\,eV\,m^2}{(35.39\times10^{-9}\,m)^2}$$

$$E_3 = 3.7\,eV + \frac{11.49\times10^{-18}\,eV\,m^2}{1252.4521\times10^{-18}\,m^2} = 3.7\,eV + 0.009\,eV \approx 3.709\,eV$$

$$E_{g,Average} = \frac{E_1 + E_2 + E_3}{3} = \frac{3.726 + 3.715\,eV + 3.709\,eV}{3} = \frac{11.15\,eV}{3} \approx 3.717\,eV$$

Calculation of Index of Refraction (n) of ITO Nano-particle

Index of refraction of ITO is given by;

$$n^4 E_g = 95\,eV \quad \Rightarrow \quad n^4 = \frac{95\,eV}{E_g} \quad \Rightarrow \quad n = \left(\frac{95\,eV}{E_g}\right)^{\frac{1}{4}}$$

$$n_1 = \left(\frac{95\,eV}{E_1}\right)^{\frac{1}{4}} = \left(\frac{95\,eV}{3.21\,eV}\right)^{\frac{1}{4}} = 2.33$$

$$n_2 = \left(\frac{95\,eV}{E_2}\right)^{\frac{1}{4}} = \left(\frac{95\,eV}{3.10\,eV}\right)^{\frac{1}{4}} = 2.35$$

$$n_3 = \left(\frac{95\,eV}{E_3}\right)^{\frac{1}{4}} = \left(\frac{95\,eV}{2.98\,eV}\right)^{\frac{1}{4}} = 2.38$$

$$n_{Average} = \frac{n_1 + n_2 + n_3}{3} = \frac{2.33 + 2.35 + 2.38}{3} = \frac{7.06}{3} \approx 2.35$$

Calculation of Dielectric Constant (k)of ITO Nano-particle

Dielectric Constant (k) is given by;

$$k = n^2$$

$$k_1 = n_1^2 = (2.33)^2 = 5.4289 \approx 5.43$$

$$k_2 = n_2^2 = (2.35)^2 = 5.5225 \approx 5.52$$

$$k_3 = n_3^2 = (2.38)^2 = 5.6644 \approx 5.66$$

$$k_{Average} = \frac{k_1 + k_2 + k_3}{3} = \frac{5.43 + 5.42 + 5.66}{3} = \frac{16.51}{3} \approx 5.50$$